

**SYNTHESIS AND CHARACTERIZATION OF  
TITANOSILICATE COMPOUNDS FOR Pb(II)  
REMOVAL**

**BY**

**WIPADA MOONKAMBIL**

**A THESIS SUBMITTED IN PARTIAL FULFILLMENT OF  
THE REQUIREMENTS FOR THE DEGREE OF MASTER OF  
ENGINEERING (ENGINEERING TECHNOLOGY)  
SIRINDHORN INTERNATIONAL INSTITUTE OF TECHNOLOGY  
THAMMASAT UNIVERSITY  
ACADEMIC YEAR 2015**

**SYNTHESIS AND CHARACTERIZATION OF  
TITANOSILICATE COMPOUNDS FOR Pb(II)  
REMOVAL**

**BY**

**WIPADA MOONKAMBIL**

**A THESIS SUBMITTED IN PARTIAL FULFILLMENT OF  
THE REQUIREMENTS FOR THE DEGREE OF MASTER OF  
ENGINEERING (ENGINEERING TECHNOLOGY)  
SIRINDHORN INTERNATIONAL INSTITUTE OF TECHNOLOGY  
THAMMASAT UNIVERSITY  
ACADEMIC YEAR 2015**



SYNTHESIS AND CHARACTERIZATION OF TITANOSILICATE  
COMPOUNDS FOR Pb(II) REMOVAL

A Thesis Presented

By  
WIPADA MOONKAMBIL

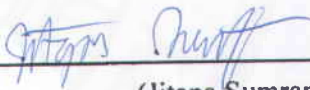
Submitted to  
Sirindhorn International Institute of Technology  
Thammasat University  
In partial fulfillment of the requirements for the degree of  
MASTER OF ENGINEERING (ENGINEERING TECHNOLOGY)

Approved as to style and content by

Advisor and Chairperson of Thesis Committee

  
\_\_\_\_\_  
(Asst. Prof. Paiboon Sreearunothai, Ph.D.)

Co-Advisor

  
\_\_\_\_\_  
(Jitapa Sumranjit, Dr.)

Committee Member and  
Chairperson of Examination Committee

  
\_\_\_\_\_  
(Assoc. Prof. Pakorn Opaprakasit, Ph.D.)

Committee Member

  
\_\_\_\_\_  
(Prof. Hirofumi Hinode, Ph.D.)

MARCH 2016

## Acknowledgements

I would like to express my sincere gratitude to so many people who have helped my thesis is greatly successful. The completion of this undertaking could not have been possible without the participation and assistance from the people following

First of all, it is my pleasure to express my deep senses of thanks to my advisor, Asst. Prof. Paiboon Sreearunothai, School of Bio-Chemical Engineering and Technology (BCET), Sirindhorn International Institute of Technology (SIIT), Thammasat University. His timely advice, scholarly advice, scientific approach, and truly sacrifice have helped my work to completely successful.

My co-advisor, Dr. Jitapa Sumranjit, the National Nanotechnology Center (NANOTEC), I am greatly thankful for giving me the helpful advice and meticulous scrutiny that are useful to my work.

I extremely grateful to Assoc. Prof. Pakorn Opaprakasit, School of Bio-Chemical Engineering and Technology (BCET), Sirindhorn International Institute of Technology (SIIT), Thammasat University. His prompt inspirations and timely suggestions with kindness have enabled me to complete my thesis.

I sincerely gratitude to Prof. Hirofumi Hinode, Tokyo Institute of Technology, whose guidance constructive criticism have contributed immensely to the evolution of my ideas on the thesis.

I also thankful to my family, friends, TAIST-Tokyo tech program, The Materials and Plasma Technology (M@P Tech) research unit, and SIIT staff who directly or indirectly have been helpful in some or the other way of my thesis.

## **Abstract**

### **SYNTHESIS AND CHARACTERIZATION OF TITANOSILICATE COMPOUNDS FOR Pb(II) REMOVAL**

**By**

**WIPADA MOONKAMBIL**

Bachelor of Science (Environmental Science), Thammasat University, 2013

Master of Engineering (Engineering Technology), SIIT, Thammasat University, 2015

Lead (Pb) is considered a highly toxic element to both human and environment. In this study, titanosilicate (TSi) compounds were synthesized and tested for removal of lead (Pb). The TSi sorbent was synthesized using sol-gel synthesis of titanium (IV)-isopropoxide (TiPO) and tetraethylorthosilicate (TEOS) mixed together with sodium hydroxide at various conditions. The adsorbents were characterized for their morphology and phases using scanning electron microscope (SEM), X-ray diffractometer (XRD), and Fourier transform infrared spectrometer (FTIR). The maximum Pb(II) adsorption capacities of the sorbents obtained are very high and in the range of 400-470 mg Pb /g sorbent. By analyzing the ratio of the released sodium ion from the sorbent to the ratio of the adsorbed Pb(II), the Pb(II) removal mechanisms are inferred to be mainly the ion-exchange. X-ray diffraction patterns show that synthesized sorbents have phases which varied from the amorphous to the crystalline states depending on synthesis condition. The sorbent in the amorphous state which prepared by the sol-gel synthesis followed by stirring at room temperature for 1h has the highest adsorption capacity. Further increase in hydrothermal time resulted in sorbent with crystalline structure, however, the sorption performance was reduced. The titanosilicate sorbents can be regenerated five times with the absorption capacity decreases 20-50%.

**Keywords:** Titanosilicate, Lead, Adsorption

## Table of Contents

Chapter	Title	Page
	Signature page	i
	Acknowledgement	ii
	Abstract	iii
	Table of contents	iv
	List of tables	vii
	List of figures	viii
1	Introduction	1
	1.1 Concept and significance	1
	1.2 Objective of the study	2
	1.3 Scope of the study	3
2	Literature Review	4
	2.1 Lead	4
	2.1.1 Properties and usage	4
	2.1.2 Accumulation	5
	2.1.3 Toxicity	6
	2.1.3.1 Effects on plants	6
	2.1.3.2 Effects on animals	6
	2.1.3.3 Effects on humans	6
	2.1.4 Problem situations	7
	2.1.5 Contaminated wastewater treatment	8
	2.2 Sorbents	13
	2.2.1 Zeolite	13
	2.2.2 Natisite (Na <sub>2</sub> TiOSiO <sub>4</sub> )	16
	2.2.3 Titanosilicate compound	18
	2.2.4 Commercial cation exchange resin	21
	2.3 Adsorption isotherm	22

2.3.1	Langmuir isotherm	23
2.3.2	Freundlich isotherm	24
2.3.3	Dubinin-Radushkevich isotherm (D-R)	25
2.4	Kinetic	26
2.4.1	Pseudo-first-order model	26
2.4.2	Pseudo-second order model	27
3	Materials and Methods	28
3.1	Reagents	28
3.2	Instruments for characterization	28
3.3	Synthesis of adsorbents	28
3.4	Lead stock solution	31
3.5	Adsorption isotherm study	31
3.6	Kinetic study	31
3.7	Regeneration	31
4	Results and Discussions	32
4.1	Synthesis of adsorbents	32
4.2	Preliminary study	32
4.3	Characterization	33
4.3.1	Scanning Electron Microscope (SEM)	33
4.3.2	X-ray Diffraction (XRD)	35
4.3.3	Fourier transform infrared (FT-IR)	37
4.3.4	Energy Dispersive X-ray spectrometer (EDS/EDX)	39
4.4	Effect of Pb (II) initial concentration	40
4.5	Effect of contact time	41
4.6	Adsorption isotherm	42
4.6.1	Langmuir isotherm	42
4.6.2	Freundlich isotherm	42
4.6.3	Dubinin-Radushkevich isotherm (D-R)	44

4.7 Kinetic study	46
4.7.1 Pseudo-first-order model	47
4.7.2 Pseudo-second-order model	47
4.8 Ion-exchange	49
4.9 Regeneration	50
5 Conclusions	57

References	58
------------	----





## List of Tables

Tables	Page
2.1 Chemical properties of lead	4
2.2 Standard and regulations on lead	8
2.3 Lead adsorption capacity on various adsorbent materials	11
2.4 Regeneration on various conditions of adsorbents	12
2.5 Properties of Lewatit® MonoPlus S 108 resin	21
3.1 Synthesis conditions of adsorbents	29
4.1 Chemical composition of adsorbents measured by The Energy Dispersive X-ray spectrometer (EDS/EDX)	39
4.2 Summary isotherm parameters for the adsorption of lead (II)	46
4.3 Summary kinetic parameters for the adsorption of lead (II)	49
4.4 Ratio of mole $Pb^{2+}$ /mole $Na^{+}$ by vary the Pb(II) initial concentration (adsorbent dose of 2g/L, room temperature, 200 rpm for 24h)	50

## List of Figures

Figures	Page
2.1 Bioaccumulation	5
2.2 Adsorption-Desorption	10
2.3 XRD patterns of zeolite by vary the hydrothermal times	13
2.4 FE-SEM images of the synthesis zeolite on various hydrothermal times	14
2.5 Four steps of the mechanism form to be the crystal zeolite in different hydrothermal times	15
2.6 X-ray diffractograms of hydrothermally prepared natisite	15
2.7 FT-IR spectra of hydrothermally prepared natisite	16
2.8 XRD pattern of (a) natisite phase using K-SiO <sub>2</sub> (b) natisite phase using n-SiO <sub>2</sub> and (c) V-Natisite	17
2.9 SEM image of prepared titanosilicates	18
2.10 XRD patterns of (a) ETS-10 prepared from TiCl <sub>3</sub> and TiO <sub>2</sub> (anatase) precursors and (b) synthesis of ETS-10 from TiCl <sub>3</sub> on various time	19
2.11 FE-SEM images of ETS-10 crystals obtained in 6 days at 200 °C from synthesis mixtures	20
2.12 SEM images of STS crystals and aggregates synthesized hydrothermally for 24 h in the system	20
2.13 Phenomena of the adsorption and desorption	22
3.1 Solid precursor	30
3.2 Hydrothermal reactor	30
4.1 Digital photograph of sorbents after drying	32
4.2 Adsorption capacity, q <sub>e</sub> (mg/g) of SP-TSi-6hΔ for preliminary study	33
4.3 SEM images: before adsorption	34
4.4 XRD patterns before adsorption	35
4.5 XRD patterns compared between before and after adsorption	36
4.6 FTIR spectra before and after adsorption	38
4.7 Effect of initial concentration (mg/L) on Pb(II) adsorption capacity, q <sub>e</sub> (mg/g) of SP-TSi-1h, SP-TSi-6hΔ, LP-TSi-6hΔ, and resin	40

4.8	Effect of contacttime (5 min-8h) on Pb (II) adsorption capacity $q_t$ (mg/g)	41
4.9	Adsorption isotherm of Pb(II) adsorption onto the four adsorbents together with fit to the Langmuir isotherm model	43
4.10	Adsorption isotherm of Pb(II) adsorption onto the four adsorbents together with fit to the Freundlich isotherm model	43
4.11	Adsorption isotherm of Pb(II) adsorption onto the four adsorbents together with fit to Dubinin-Radushkevich isotherm model	44
4.12	Pseudo-first-order kinetic model for the adsorption of Pb(II) onto the synthesized adsorbents	47
4.13	Pseudo-second-order kinetic model for the adsorption of Pb(II) onto the synthesized adsorbents	48
4.14	Adsorption capacity, $q_e$ (mg/g) of SP-TSi-1h, SP-TSi-6h $\Delta$ , and LP-TSi-6h $\Delta$ after regeneration on various conditions	51
4.15	Adsorption capacity, $q_e$ (mg/g) of SP-TSi-6h $\Delta$ after regenerated by 4M NaOH for 2, 4, and 24h	51
4.16	Adsorption capacity at equilibriums, $q_e$ (mg/g) depend on the number of cycle regeneration	52
4.17	FTIR spectra compare between after adsorption and after reuse of SP-TSi-1h, SP-TSi-6h $\Delta$ , and LP-TSi-6h $\Delta$	53
4.18	Pb(OH) <sub>2</sub> preparation (a) added by 5M NaOH, (b) after centrifuge, and (c) DI water	54
4.19	FTIR spectra of Pb(OH) <sub>2</sub>	55
4.20	FTIR spectra compare between Pb(OH) <sub>2</sub> and the adsorbents after reuse	56

# Chapter 1

## Introduction

### 1.1 Concept and Significance

Currently, lead is used in many industries such as electronics, batteries, plastic container coating, and mine processing. Lead is a highly toxic element than can adversely affect many parts of the body, particularly central nervous system. It can also retard mental development in children [1, 2]. As a result, a number of federal agencies have issued advisory standards or enforceable regulations that set maximum permissible lead levels in different media. For instance, in Thailand, the Industrial Effluent Standards set by Pollution Control Department (PCD) dictates that the concentration of lead cannot be more than 0.2 mg/L [3] and the maximum concentration of lead in drinking water according to the Environmental Protection Agency cannot be more than 15 µg/L [4]. The basic treatment for lead removal in industries is usually by chemical precipitation by adjustment to alkaline pH (pH 9–11) [4] where lead ion will be precipitated into lead hydroxide. However, this process requires large amount of chemicals and often the final colloidal lead hydroxide is difficult to be separated from the treated water. Adsorption is one of the attractive treatment techniques for lead removal due to its simplicity, reusability, easy separation, and also with potential for metal recovery [5]. Many adsorbents have been tested and used for removal of lead from contaminated water such as those from agricultural and biological wastes, natural zeolite, and biopolymers including also their various functionalization. The reviews of lead removal are shown in M.A. Barakat (2011) [4]. The range of maximum capacity between 1.6-235 mg/g.

Previously, zeolite, a crystalline aluminosilicates which has structure based on tetrahedral  $\text{SiO}_4$  and  $\text{AlO}_4$  units [6] is used as adsorbents because it has high selectivity for certain heavy metal ions and coated with others material for improving their ability. Synthesized zeolite tends to have more uniform properties and possess high ion exchange capacity than their natural counterparts. One variation of zeolite known as titanosilicate, which is constructed from network of  $\text{TiO}_6$  and  $\text{SiO}_4$  building unit, has been shown to have many interesting novel properties such as catalysis, molecular sieve, and ion exchange properties. L. Lv et al. (2005) [7] have reported the use of one

type of crystalline titanosilicate materials (ETS10) which can adsorb about 300 mg Pb/g sorbent. However, the synthesis of these ETS10 crystalline titanosilicates took many steps and long synthesis time of about 60h. The synthesis of crystalline titanosilicate usually carried over via the sol-gel process followed by hydrothermal treatment which involves long synthesis time from several hours up to several days [8]. For instance, G.-W. Peng. and H.-S. Liu (1995) [9] reported the titanite synthesized by using  $\text{SiO}_2$  and  $\text{Ti}_4$  [8] in ratio 1:1 mixed with NaOH. The mixture was heated in hydrothermal at  $200^\circ\text{C}$  for 30h.

In this work, a highly efficient Pb sorbent has been developed based on titanosilicate compounds using facile sol-gel synthesis coupled with partial hydrothermal treatment in order to reduce synthesis time. The sorbent was then tested for their Pb sorption performance using batch mode and found to have high Pb sorption capacity with the maximum one of 430 mg Pb/g sorbent. The morphology, phase and surface area of these sorbents were also investigated using x-ray diffraction, and scanning electron microscope. It was found that partial hydrothermal treatment was beneficial in Pb sorption due probably to increased porosity while further increase in hydrothermal time decreased the sorption performance, due probably to the rigid crystalline structure. A simple and easy synthesis of titanosilicate has been employed in this work.

## **1.2 Objectives of Study**

- 1.2.1** To synthesize and characterize properties of adsorbent materials; titanosilicate compounds.
- 1.2.2** To investigate the removal efficiency of Pb using synthetic wastewater by the titanosilicate sorbents in batch experiment.
- 1.2.3** To study the adsorption mechanisms of Pb on surface of the titanosilicate sorbents.
- 1.2.4** To explore the efficiency of using sodium hydroxide to regenerate and reuse titanosilicate sorbents.

### **1.3 Scope of Study**

Titanosilicate used as Pb removal materials are prepared by hydrothermal reaction. The Scanning Electron Microscopy (SEM) was employed to examine surface morphology and the Energy Dispersive X-ray Spectrometer (EDS/EDX) analyze the chemical compositions of titanosilicate materials before and after adsorption. The X-ray Diffraction (XRD) was carried out in order to determine the structural change after Pb adsorption, compared to those before adsorption. The batch adsorption experiments were conducted to study the adsorption mechanism of Pb by employing FT-IR spectroscopy. The concentration of Pb solution were measured by inductively coupled plasma-atomic emission spectroscopy (ICP-OES). The regeneration of sorbent was investigated using DI water and NaOH.

## Chapter 2

### Literature Review

#### 2.1 Lead

##### 2.1.1 Properties and Usage

Lead is an element with the symbol of “Pb”. It is a soft, highly malleable, ductile, and heavy post-transition metal [10]. The properties of lead and lead nitrate which are commonly used to prepare the stock solution are shown in **Table 2.1**. Nowadays, lead has grown to become a major elemental pollutant because of its usage in various industries as raw materials such as solder, glass, pottery glazes, rubber, plastics, paints, and insecticide [11]. The properties of lead which make it a favorite choice for use in many applications are malleability, ductility, softness, and resistance to corrosion.

**Table 2.1 Chemical Properties on Lead [12]**

Property	Lead	Lead nitrate
<b>Molecular weight</b>	207.20 g/mol	331.21 g/mol
<b>Color</b>	Bluish-gray	Colourless or white
<b>Physical state</b>	Solid	Solid
<b>Melting point</b>	327.4 °C	Decomposes at 470 °C
<b>Boiling point</b>	1,740 °C	No data
<b>Density at 20 °C</b>	11.34 g/cm <sup>3</sup>	4.53 g/cm <sup>3</sup>
<b>Solubility Water at 25 °C</b>	Insoluble	376,500 mg/L at 0 °C, 565,000 mg/L at 20 °C
<b>Vapour pressure</b>	1.77 mmHg at 1,000 °C	No data
<b>Valence state</b>	0	+2

### 2.1.2 Accumulation

There are many sources of lead in the environment such as the household paint, industry effluent, emission gases, mine processing and hazardous waste. Lead can be released to the main phases of the ecosystem: atmosphere, water, food, living organism, and soil. **Figure 2.1** presents the bioaccumulation of lead when released into the ecosystem.

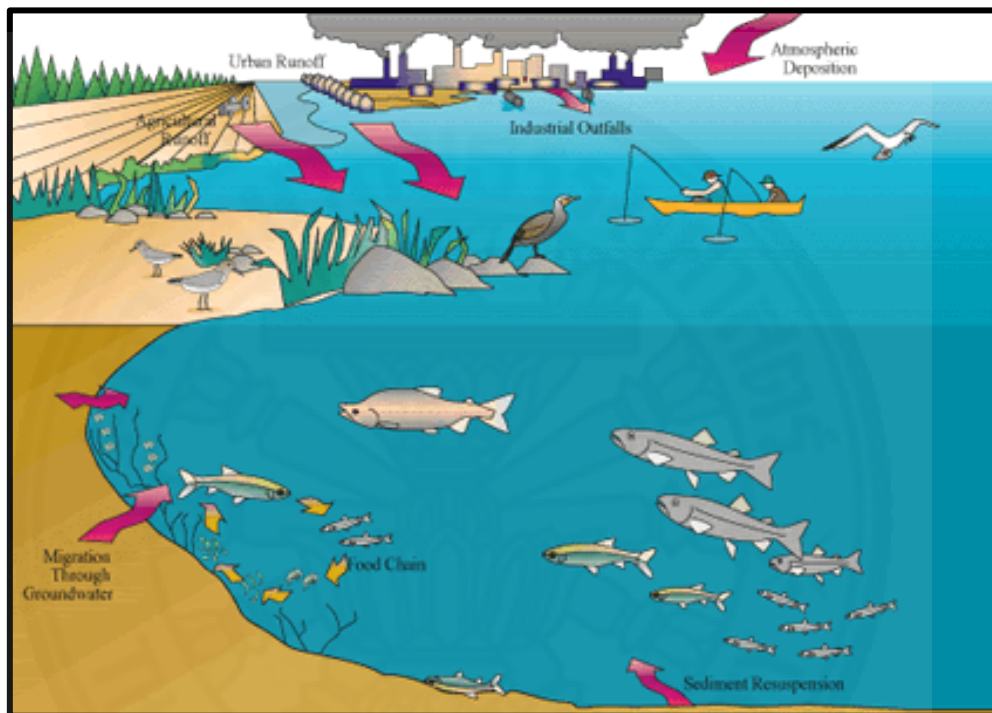


**Figure 2.1 Bioaccumulation** [13]

In ambient air, lead is released from gaseous emission and smoke-stack. In addition, the major sources of lead contamination in air are the exhaust from automobiles. The synthesized tetraethyl lead, (TEL  $\text{Pb}(\text{C}_2\text{H}_5)_4$ ), is for used increasing the octane number of gasoline. TEL is then combusted into lead oxide ( $\text{PbO}$ ) which become an atmospheric pollutant [14]. The deposition of lead from polluted air, hazardous waste leachate, and insecticide can be accumulated by water from snowmelt, rainfall, and irrigation runs through the ground into a soil. The runoffs takes the pollutants lead directly into the river or ocean. In aquatic ecosystems which have several micro-organisms including fungi, plankton, bacteria, and protozoans. They consume the sediment where the lead precipitate to the bottom and then the toxic lead can enter into the food chain. Finally, the top consumer, humans takes into the body and affect their health.



### **2.1.3 Toxicity**

#### **2.1.3.1 Effect on Plants**

The behavior of lead on plants, the phytotoxicity significantly depends on the species of chemical speciation. They can be form organo-metallic complex by organic ligands which can modify lead speciation efficiently. Organic ligands efficiency modify lead behavior mainly depend on the metal binding capacity of them. This depends on amount, molecular structure, and functional groups of organic ligand types [15]. The study of effect lead on bush bean report that roots uptake of lead in the soil pore and accumulate on the seed, leaves, stems, and pods. The previous researches report the effect of lead on plants [16]. They study lead uptake of tea plant that grown on a lead contaminated soil for three years. The results show that the biomass decrease significantly as concentration of lead increased and phytotoxic symptoms appear [17].

#### **2.1.3.2 Effect on Animals**

Fish is a good bioindicator for the lead accumulation because it consumes a micro-organism and contaminated sediment in the aquatic ecosystem. Recently, the study effect of lead in fish presents that lead is accumulated in the gills, liver, and muscle. Gill is the major path that the metal can be exchanged ion from water because it has the large surface areas to facilitate rapid diffusion of pollutant [18]. Furthermore, lead also accumulate in the egg and eggshell of fish [19].

#### **2.1.3.4 Effect on Humans**

The study of lead toxicity in newborns reports that pregnant women and children possibly absorb over 40% of consumed lead. It is a high risk in newborns. The blood lead levels in newborns are usually more than their mother levels as a result of the simple diffusion and unidirectional route of lead across the placenta. The primary pathways of lead that can enter to the body are ingestion, inhalation, and placental transfer. It can be absorbed, exchanged, and distributed in the hematologic, soft tissue, and mineralizing tissue compartments. Bone formation can be changed because of lead consumption. High levels of lead alter the cellular processes in calcium-binding protein

which is the synthesis of osteoblastic bone cells. Lead affects many organ systems and the effect on developing nervous systems of children is the most significant. Lead also interferes synaptic neurotransmitters and their receptors, resulting in the symptoms of distractibility, impulsivity, coma, and even death [20]. Another work confirm lead as a carcinogen. The carcinogenicity of lead compounds has been studied because of continuing environmental sources of exposure. Lead toxicity in several target organs, especially the nervous system, for this results, lead carcinogenic mechanisms remain mainly unknown. Lead possibly facilitate genetic damage through several mechanisms. These include inhibition of oxidative damage, DNA synthesis and repair, and interaction with DNA-essential proteins and neoplasm suppressor proteins [21].

#### **2.1.4 Problem Situations**

In China, there is a study of bioaccumulation of lead in the Pearl River. The Pearl River discharged heavy metals to the Mai Po Ramsar site which is the largest wetland in Hong Kong, and caused environmental deterioration. A study report that the high concentration of lead is found in the bodies of, the top consumer in the wetland ecosystem which are the waterbirds. Muscles, eggs, and eggshells are also reported to have the lead accumulation [19]. In Egypt, the Red Sea is an important ecosystem to study the bioaccumulation of lead because population growth and industrial activities have increased in the north part. The results show that lead accumulates in fish muscles [18].

In Thailand, an interested case about lead contaminate to the environment is the Klity creek which are located in the west of Thailand, Kanchanaburi province. It is one of water resources of the main Meklong River of the western region of Thailand. Lead were released to the creek since 1990 due to the lead mine processing. The toxins leak into the Lower Klity Creek Watershed [22]. This affects the plants, animals, and people who live in this village. The locals, the ethnic Karen people, have used the creek as water resource in daily activity such as bathing, fishing, drinking, cooking and everything involving water. The villagers began to symptom head aches and pain in their bones. However, the children and pregnant women were at most risk in this situation. Lead poisoning affects to pregnant women would often miscarry and develop learning handicap. In 1998, the Thai government inspected the villager's health and

found lead contamination in their blood. The Pollution Control Department (PCD) of Thailand had apathetic attitude to remove lead from the village's creek and had no plans to restore the creek. In 2003, the locals took PCD to court. The court found that the PCD had been ignorant in cleaning the creek. The court ordered the PCD to pay the fine. PCD evidently has begun the restoration of Klity Creek by October 2015 [23]

### 2.1.5 Contaminated Wastewater Treatment

Lead is an important cause that effects to the public health problems. So a number of federal agencies have issued advisory standards and enforceable regulations which set the levels of lead in different media. **Table 2.2** summarized standards and regulations [24].

**Table 2.2 Standard and Regulations of Lead**

Agency	Media	Level	Comments
CDC	Blood	10 µg/dL	Advisory; level for individual management
OSHA	Blood	40 µg/dL	Regulation; cause for written notification and medical exam
		60 µg/dL	Regulation; cause for medical removal from exposure
ACGIH	Blood	30 µg/dL	Advisory; indicates exposure at the threshold limit value (TLV)
OSHA	Air (workplace)	50 µg/m <sup>3</sup>	Regulation; PEL (8-hr average.) (general industry)
		30 µg/m <sup>3</sup>	Action level
CDC/NIOSH	Air (workplace)	100 µg/m <sup>3</sup>	REL (non-enforceable)
ACGIH	Air (workplace)	150 µg/m <sup>3</sup>	TLV/TWA guideline for lead arsenate
		50 µg/m <sup>3</sup>	TLV/TWA guideline for other forms of lead

**Table 2.2 Standard and Regulations of Lead**

<b>Agency</b>	<b>Media</b>	<b>Level</b>	<b>Comments</b>
<b>EPA</b>	Soil (residential)	400 ppm (play areas) 1200 ppm (non play areas)	Soil screening guidance level; requirement for federally funded projects only (40 CFR Part 745, 2001)
<b>EPA</b>	Air (ambient)	0.15 µg/m <sup>3</sup>	Regulation; NAAQS; 3-month average
<b>EPA</b>	Water (drinking)	15 µg/L 0 µg/L	Action level for public supplies Non-enforceable goal; MCLG
<b>FDA</b>	Food	Various	Action levels for various foods; example: lead-soldered food cans now banned
<b>CPSC</b>	Paint	600 ppm (0.06%)	Regulation; by dry weight. There is a new standard for lead in children's jewelry.
Notes			
CDC	:	Centers for Disease Control	
OSHA	:	Occupational Safety and Health Administration	
ACGIH	:	American Conference of Governmental Industrial Hygienists	
NIOSH	:	National Institute for Occupational Safety and Health	
EPA	:	Environmental Protection Agency	
FDA	:	Food and Drug Administration	
CPSC	:	Consumer Product Safety Commission	

From: Agency for Toxic Substances and Disease Registry (2012)

According to the standards, a pollutant should be treated before discharging. This work focus on the lead contaminated in water, especially, effluent from industry. Normally, there are several common methods are used to remove lead from wastewater such as chemical precipitation, adsorption, ion exchange, coagulation, and flocculation. The advanced methods are also applied such as membrane filtration and electrochemical treatment. However, the two methods that widely used in industry are chemical precipitation and adsorption.

Chemical precipitation is generally used to remove lead from the industry effluent especially wastewater that contaminate with a large amount of inorganic. Adjustment of pH between 9 and 11 is basic conditions that greatly improves lead removal by chemical precipitation. Common chemicals are used in the precipitation processes which are sodium hydroxide and lime and others coagulants such as organic polymers, alum, and iron salts. Chemicals react with the lead ions and produce the precipitates. Then, the sedimentation can help the precipitates separated from the water and treated water before discharged or reused. The advantages of chemical precipitation process are effective at high lead concentration, inexpensive cost, and simple process. For the disadvantage, this technique require the final disposal because it produces a large amount of sludge and cause the long-term environmental impacts [4, 5].

For this results, adsorption become a recognized method for removing lead from contaminated wastewater in term of an effective and economic. The general definition describes adsorption mechanism is a mass transfer process. Firstly, the ions in the liquid phase are transferred to the solid surface. Then, they bound the physical and/ or chemical interactions. In addition, adsorption includes the process of precipitation. The basic terms are shown in **Figure 2.2**. The solid materials that provide the surface area for adsorption is called adsorbent. The adsorbate is the species that will be adsorbed. On the other hand, the reverse process can occur when the adsorbed are released from the surface of solid and transferred back into the liquid phase by changing the properties of the liquid phase. The reverse process is called desorption.

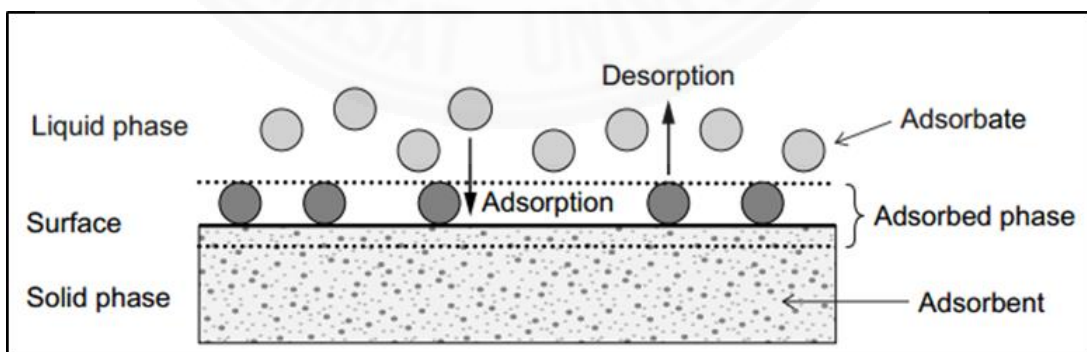


**Figure 2.2 Adsorption-Desorption**

**Table 2.3 Lead adsorption capacity on various adsorbent materials**

<b>Sorbent materials</b>	<b><math>q_{\max}</math> (mg of Pb / g of adsorbent) by Langmuir Isotherm</b>	<b>Conditions</b>	<b>Ref.</b>
activated carbons from lignocellulosic	50-112	30°C, pH 5	[25]
mesoporous magnetite (Fe <sub>3</sub> O <sub>4</sub> ) nanospheres	18	45°C, pH 5	[26]
Zeolite (Z) and Montmorillonite (Mt)	50-115	room temperature, pH 7	[27]
energy cane biochars	40-70	25-45°C, pH 5	[28]
hierarchical MgFe <sub>2</sub> O <sub>4</sub> microspheres	113	room temperature, pH 7	[29]
zeolite-NaX	14	30°C, pH 6	[30]
Large-pore diameter nano-adsorbent	169	25°C, pH 5.2	[31]
Tamarind wood activated carbon	134	room temperature, pH 6.5	[32]
magnetic carbon nanotubes/diatomite	60	room temperature, pH 6	[33]
sawdust activated carbon	43-116	30°C, PH 2-8	[34]
polysiloxane-graphene oxide gel	222-256	20-40°C. pH 5	[35]
xanthate-modified magnetic chitosan	77	25°C, pH 5	[36]
Polygonum orientale Linn activated carbon	98	25°C, pH 5	[37]
multi-walled carbon nanotubes	7	30°, pH 7	[38]
magnetic chitosan hydrogel beads	134-175	25°C, PH 4.5	[39]

Many varieties of adsorbent materials have been developed and applied for lead removal from contaminated wastewater such as natural material, agricultural, modified biopolymers, and industrial waste. However, the efficiency of adsorption depends on the type of adsorbents which shows in **Table 2.3**.

**Table 2.4** shows the sample of adsorbent that can be generated by various conditions. In term of economy, cost-effectiveness and technical applicability are the main reason to select the most suitable adsorbent for removal of lead. Because sometime the adsorption process can be reversed and adsorbents can be reuse by regeneration with the appropriate desorption process.

**Table 2.4 Regeneration on various conditions of adsorbents**

Sorbent materials	% Recovery	Cycles	Reagents	Ref.
Hierarchical MgFe <sub>2</sub> O <sub>4</sub> microspheres	98-100	2	0.1N HCL, 10 ml	[28]
Large-pore diameter nano-adsorbent	97	7	0.3M HCL	[31]
Polysiloxane-graphene oxide gel	90–95	6	0.1–1.0M HNO <sub>3</sub>	[35]
Carboxylated cellulose nanofibrils-filled magnetic chitosan hydrogel beads	90	4	0.01 M HNO <sub>3</sub>	[39]
Chitosan-based granular	90	5	0.5M acid group	[40]
Carbon foam	70	5	0.1 N HNO <sub>3</sub>	[41]
Nanoalginate based biosorbent	98	4	0.0001-0.1M HCL	[42]
Novel nano-mineral	20-90	4	1M NaCl+ 1M NH <sub>4</sub> OH	[43]
Core–mesoporous shell silica spheres	98–99	4	3M HNO <sub>3</sub>	[36]
Magnetic graphene composite	80	5	0.2M NaOH + 0.01M HCL	[44]

## 2.2 Sorbents

### 2.2.1 Zeolite

Zeolites are widely used as adsorbent and are normally synthesized by using the hydrothermal reaction in alkaline aqueous solutions. The synthesis conditions rely on the desired composition of the materials such as particle size and morphology. The most hydrothermal temperatures are between 100-300 °C at the corresponding low solution vapor pressure are applied. The slurry consisting of hydroxide and oxide is fed into the autoclave. This mixture is heated at preferred reaction temperature. Primarily, the slurry reacts through dissolution, precipitation forming stable compound. After heating, the autoclave is cool, the product can be separated by filtration and washed several times. [45]

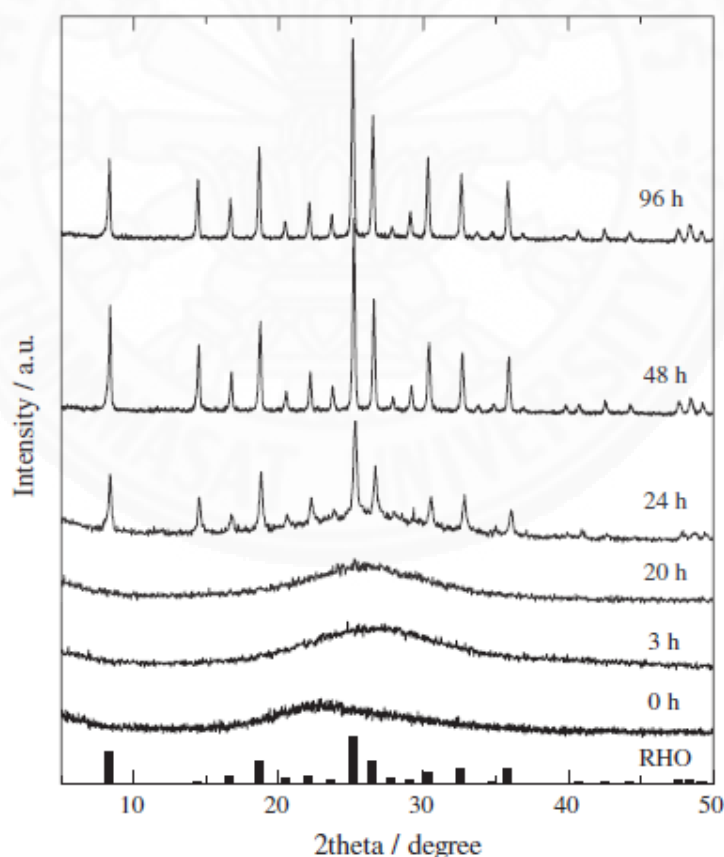
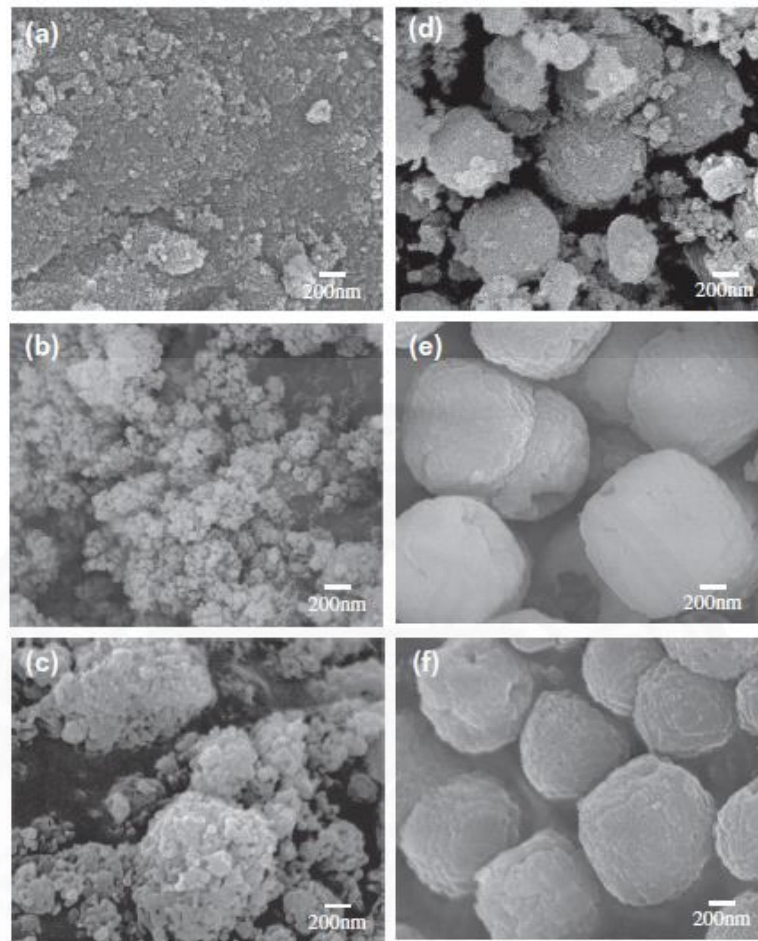


Figure 2.3 XRD patterns of zeolite by vary the hydrothermal times [46]





**Figure 2.4 FE-SEM images of the synthesis zeolite on various hydrothermal times: (a) 0 h, (b) 3 h, (c) 20 h, (d) 24 h, (e) 48 h, and (f) 96 h [46]**

S. Araki et. al (2012) report four steps to synthesis zeolite which depends on hydrothermal time (0-96 h at 110 °C). The results show XRD patterns (**Figure 2.3**) that no peaks on the condition of 0, 3, and 20 h. After 24 h, the peaks appeared and become sharper with increased in the treatment time. The XRD patterns are consistent with the FE-SEM images where the particle size grows with the increasing hydrothermal time (**Figure 2.4**).

Four steps of forming zeolite were proposed, firstly at 0-3 h, the dehydration and condensation reactions between alumina and silica form to be the amorphous aluminosilicates compounds. Secondly at 3–20 h, the amorphous aluminosilicate particles growth and aggregation. After that at 20-48 h, the particles growth to be the crystal zeolite by crystallization process. Finally, after 48 h, gentle growth. For each process, the Si/Al, Na/Si, and Cs/Si ratio affect to the bonding (**Figure 2.5**).

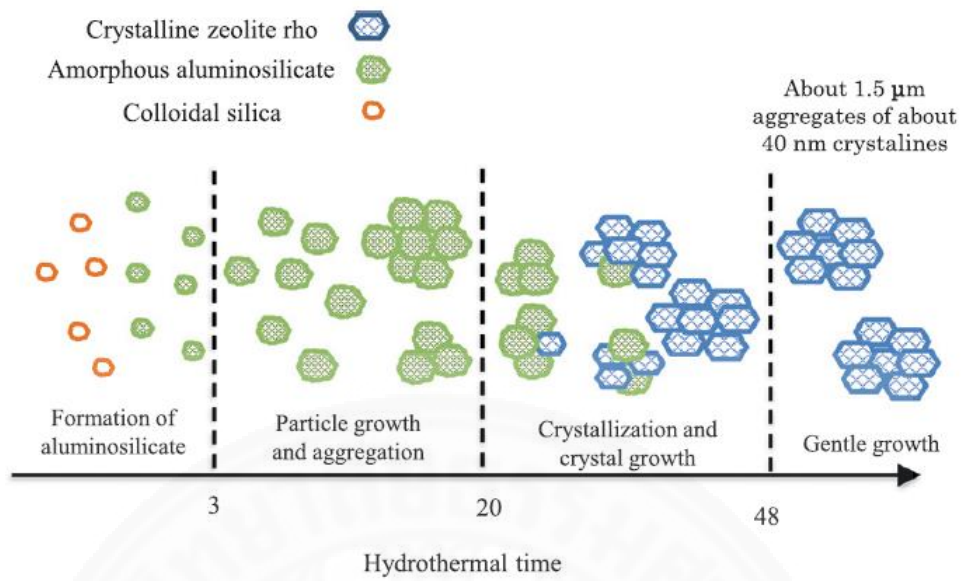


**Figure 2.5** Four steps of the mechanism form to be the crystal zeolite in different hydrothermal time [46]

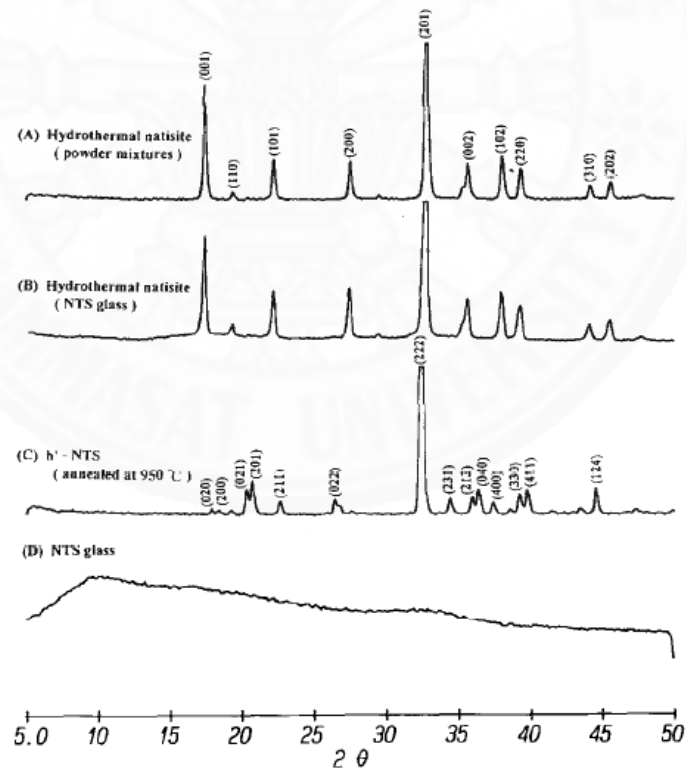


**Figure 2.6** X-ray diffractograms of the hydrothermally prepared natisite: (a) powder mixture ( $\text{Ti}(\text{OH})_4/\text{SiO}_2$ ); (b)  $\text{Na}_2\text{O}-\text{TiO}_2-\text{SiO}_2$  (NTS) glass; (c) low ( $h'$ )-NTS ( $\text{Na}_2\text{TiSiO}_5$ ) phase from annealed NTS glass; (d) NTS glass [9]

### 2.2.2 Natisite ( $\text{Na}_2\text{TiOSiO}_4$ )

A sodium titanium silicate polycrystalline powder, natisite ( $\text{Na}_2\text{TiOSiO}_4$ ) which is can be grown by a hydrothermal reaction [9]. **Figure 2.6** presents the XRD patterns of natisite on different preparation. **Figure 2.6** (a) and (b) shows that the strong peaks are located at  $2\theta = 32^\circ$  and during phase transformation of natisite. The FT-IR spectrometer is used to identify the functional group that shown in **Figure 2.7**.

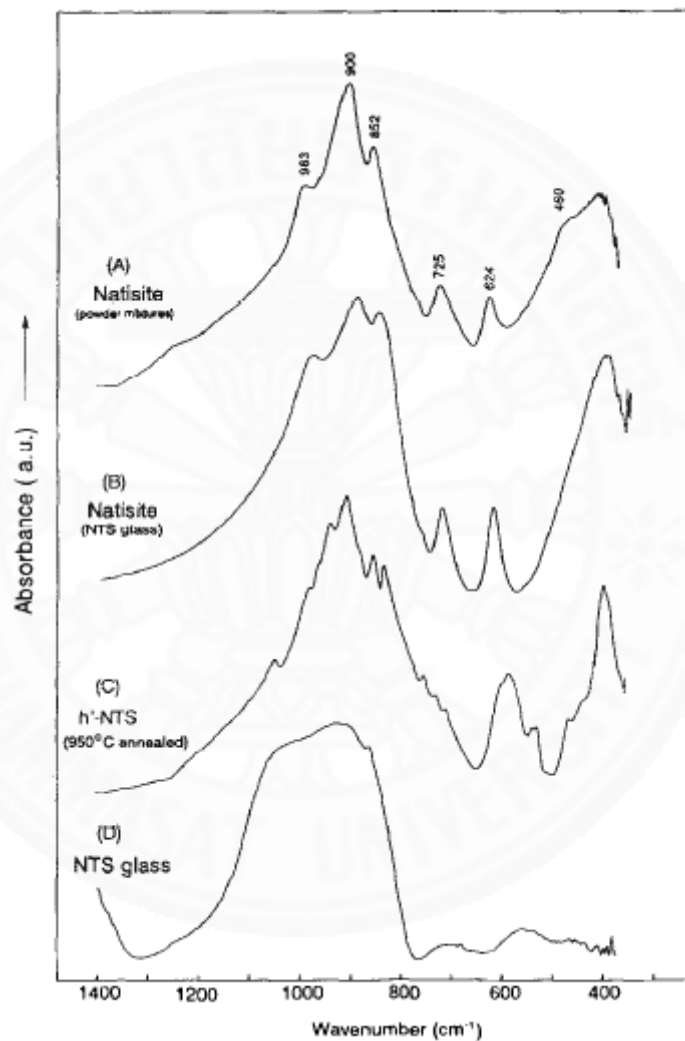


**Figure 2.7** FT-IR spectra of hydrothermally prepared natisite: (a) powder mixture ( $\text{Ti}(\text{OH})_4/\text{SiO}_2$ ) ; (b)  $\text{Na}_2\text{O}-\text{TiO}_2-\text{SiO}_2$  (NTS) glass; (c) low (h')-NTS ( $\text{Na}_2\text{TiSiO}_5$ ) phase from annealed NTS glass; (d) NTS glass [9]

The results show two IR spectra of (a) and (b) quite similar which two relatively sharp bands at 725 and 624  $\text{cm}^{-1}$  and two broad bands at 1200-750 and 560-360  $\text{cm}^{-1}$ . Spectrum (C) shows a very broad band that represents the low NTS phase

and two smaller bands show in the ranges of 640-350 and 490-350  $\text{cm}^{-1}$ . In addition, amorphous phase are appeared in spectrum (d). This work was successful to synthesis natisite under hydrothermal process at 200  $^{\circ}\text{C}$  for 24h. Another study, natisite are synthesized by white sand silica source from Red Sea Desert mine. The Si and Ti sources are mixed with NaOH and transfer to Teflon-lined stainless steel autoclave. The mixture were treated at 200  $^{\circ}\text{C}$  for 24h [47].

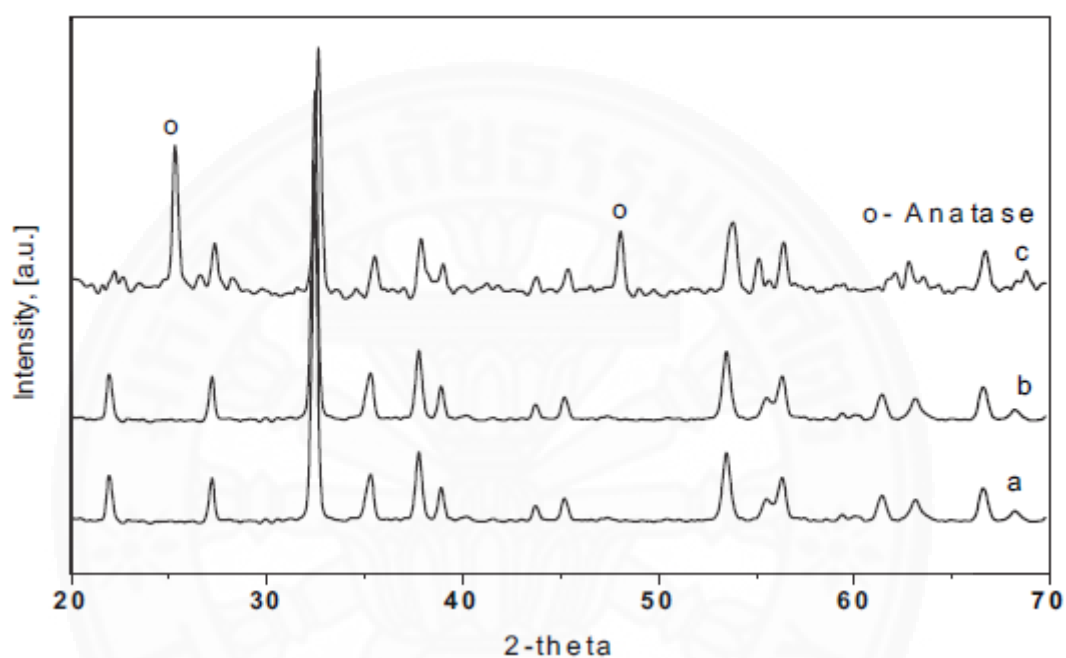


**Figure 2.8** XRD pattern of (a) natisite phase using  $\text{K-SiO}_2$  (b) natisite phase using  $\text{n-SiO}_2$  and (c) V-Natisite [47]

**Figure 2.8**, it is found that the XRD patterns consist of all diffraction lines of well crystallized pure tetragonal natisite and the same positions of the strong peak in previous study [9] which is 32  $^{\circ}\text{C}$ . In addition, it has no reactants left unreacted. Meanwhile the images from SEM show the morphology (**Figure 2.9**). Images (a) show aggregated plate, (b) are shaped grains, (c) look like plant leaves, (d) appear cuboids shape, (e) identify cubic microstructure, and (f) refer to sponge shape. Obviously, the different sources of silica precursor effect the structures of the same type of titanosilicate.

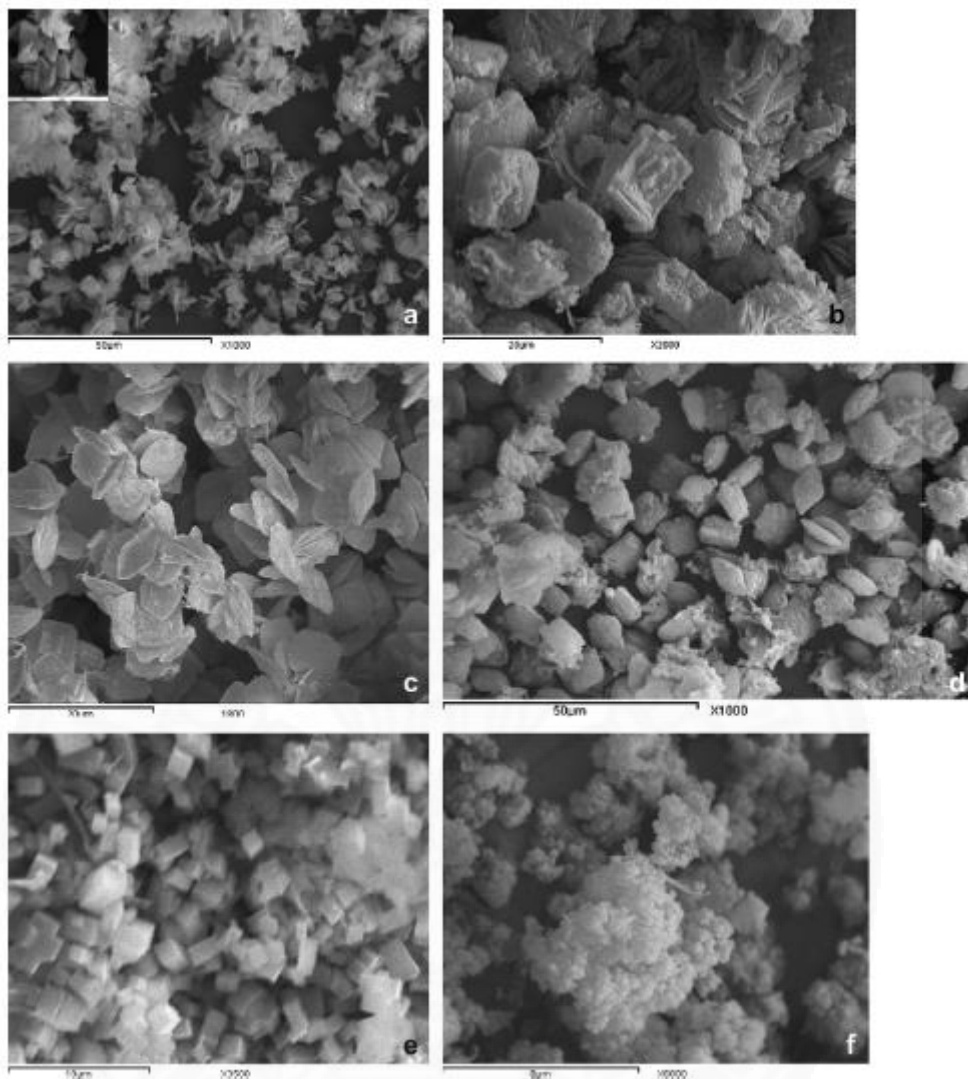


**Figure 2.9 SEM image of prepared titanositicates, (a) ETS-4; (b) V-ETS-4; (c) Natisite prepared by K-SiO<sub>2</sub>; (d) natisite prepared by n-SiO<sub>2</sub>, (e) sitinakite prepared by K-SiO<sub>2</sub>; (f) Sitinakite prepared by n-SiO<sub>2</sub> [47]**

### **2.2.3 Titanosilicate compound**

J. Rocha et al. (1998) [48] present the hydrothermal synthesis conditions of Engelhard titanosilicate (ETS) which is a novel large-pore titanosilicate consist of titanium dioxide (TiO<sub>2</sub>). This process shows the comparison between 2 precursors which is titanium trichloride (TiCl<sub>3</sub>) and TiO<sub>2</sub> (anatase). Homogenous gel was formed and treated at 230°C for 24 h in Teflon-lined autoclaves. The gel composition was 4.7Na<sub>2</sub>O:1.5K<sub>2</sub>O:TiO<sub>2</sub>:5.5SiO<sub>2</sub>:122H<sub>2</sub>O which is close to (Na<sub>1.5</sub>, K<sub>0.5</sub>) TiSi<sub>5</sub>O<sub>13</sub>. The asterisks depict the reflection given by anatase (**Figure 2.10 (a)**). The treatment

hydrothermal time are varied (3-72 h). The XRD results indicate the beginning of the amorphous phase. After that, some ETS-10 began to form the crystalline when synthesis time more than 6 h. (**Figure 2.10 (b)**).

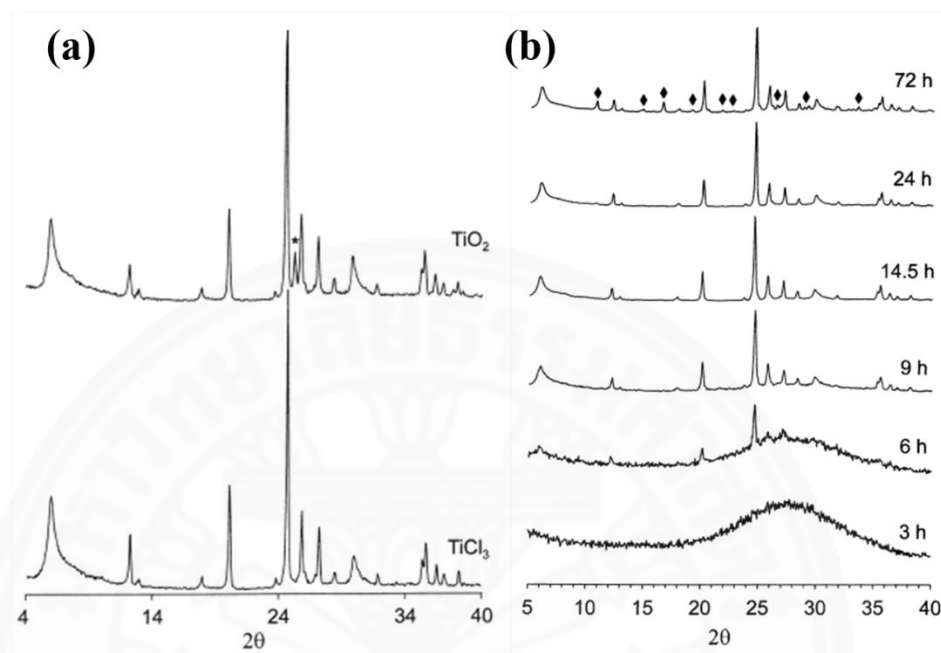


**Figure 2.10 XRD patterns of (a) ETS-10 prepared from  $\text{TiCl}_3$  and  $\text{TiO}_2$  (anatase) precursors and (b) synthesis of ETS-10 from  $\text{TiCl}_3$  on various time [48]**

The precursor  $\text{TiCl}_3$  in previous study present problem because it is high sensitivity to air and humidity [49]. In 2005, Z. Ji et al. used  $\text{Ti}(\text{SO}_4)_2$  as Ti source to synthesize ETS-10 under hydrothermal treatment at  $200^\circ\text{C}$  for 4–10 days [50]. When focus the effect on the  $\text{Na}_2\text{O}$ ,  $\text{SiO}_2$ , and  $\text{TiO}_2$  ratios, the size and morphology are shown in **Figure 2.11**. Increasing of  $\text{Na}_2\text{O}/\text{SiO}_2$  ratio in the mixture can clearly find that ETS-10 crystals become flatter. The study effect of Ti content are reported in V. Kostov-Kytin et al. (2007) [51]. The formation of large single crystals are observed when increase the Ti content in the initial gel. The micro-crystals growth arrangement forms spherical ball that is presented in **Figure 2.12**.

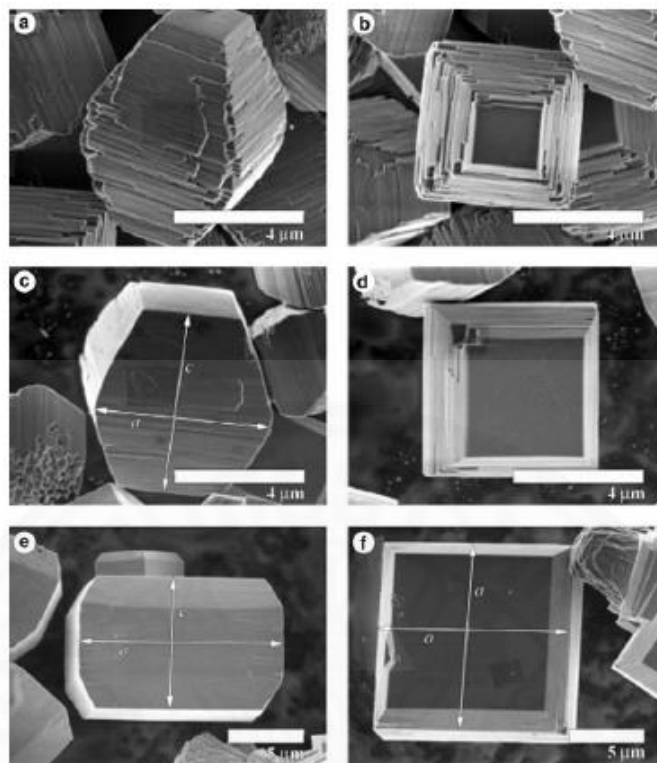


**Figure 2.11** FE-SEM images of ETS-10 crystals obtained in 6 days at 200 °C from the synthesis mixtures with  $\text{SiO}_2/\text{TiO}_2 = 5.50$ ,  $\text{KF}/\text{TiO}_2 = 1.5$ ,  $\text{H}_2\text{O}/\text{TiO}_2 = 300$ , and (a, b)  $\text{Na}_2\text{O}/\text{SiO}_2 = 0.790$ ; (c, d)  $\text{Na}_2\text{O}/\text{SiO}_2 = 0.840$ ; (e, f)  $\text{Na}_2\text{O}/\text{SiO}_2 = 0.930$  [50]

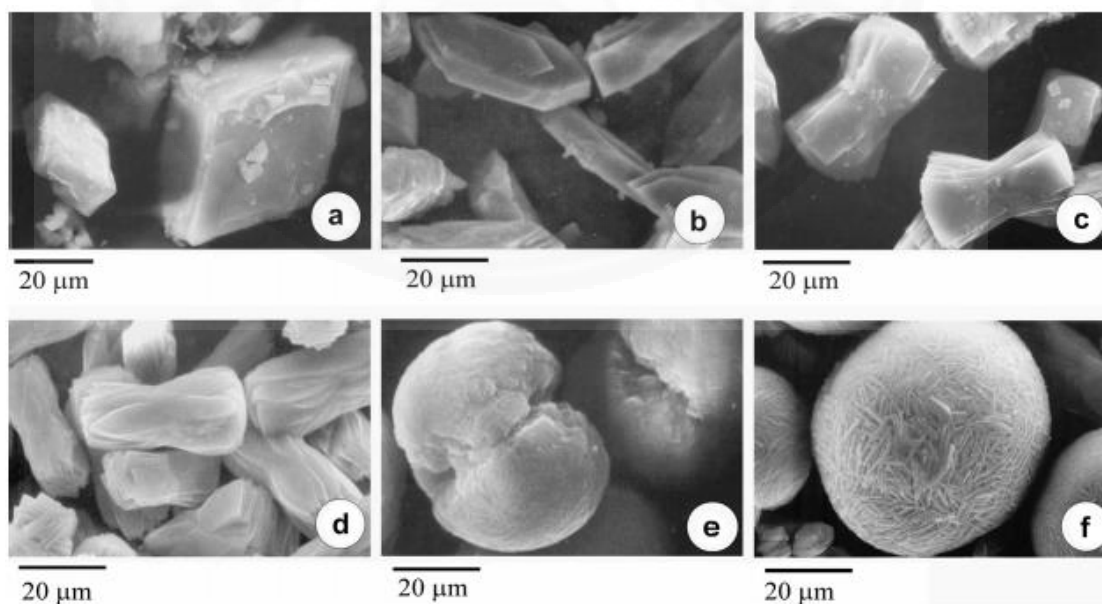


**Figure 2.12** SEM images of titanosilicate crystals and aggregates synthesized hydrothermally for 24 h in the system  $2\text{Na}_2\text{O}-7\text{K}_2\text{O}-c\text{TiO}_2-10\text{SiO}_2-675\text{H}_2\text{O}$ , where: (a)  $c = 0.3$ ; (b)  $c = 0.6$ ; (c)  $c = 0.9$ ; (d)  $c = 1.2$ ; (e)  $c = 1.5$ ; (f)  $c = 1.8$  [51]

### 2.2.4 Commercial cation exchange resin

Lewatit<sup>®</sup> MonoPlus S 108 is the cation exchanger resin in monodisperse uniform size which is made of a styrene-divinylbenzene copolymer. This resin type is specially manufactured to be strongly resistant to chemical, and mechanical stress. These result in low leachable even though under the critical conditions such as higher temperatures, oxidation, and external regeneration processes. In addition, it is very short regeneration times. The properties of the resin are list in **Table 2.5**.

**Table 2.5 Properties of Lewatit<sup>®</sup> MonoPlus S 108 resin [52]**

Properties	Description	Unit
<b>General</b>		
Ionic form as shipped	Na <sup>+</sup>	
Fuctional group	Sulfonic acid	
Matrix	Crosslinked polystyrene	
Structure	Gel type beads	
Appearance	Black-brown	
<b>Physical and chemical</b>		
Mean bead size	0.62 (±0.05)	mm
Density	1.30	Approx.. g/ml
Total capacity	2.2	Min. eq/L
Volume change Na <sup>+</sup> → H <sup>+</sup>	10	Max. vol.%
Stability at pH-range	0-14	
Storability of the product	2	Max. years
Storability temperature range	-20 – 40	°C
<b>Recommended Operating Conditions</b>		
Operating temperature	20	°C
Operating pH range	0-14	
Regenerant	HCl, H <sub>2</sub> SO <sub>4</sub> , NaCl	



### 2.3 Adsorption Isotherm

Equilibrium relationships between sorbates and sorbents can be explained by sorption isotherms in the form of  $Q = f(C)$ . It can find the sorption capacity of a sorbent. **Figure 2.13** shows the phenomena of the adsorption and desorption. The final concentration on the solid phase ( $Q$ ) can be calculated by the difference between the initial concentration in liquid phase ( $C_{a_0}$  or  $C_{b_0}$ ) and the concentration remaining in liquid phase after adsorption ( $C$ ). Adsorption equilibrium data indicates the relationship between mass of adsorbate is adsorbed and adsorbent in weight unit. The adsorption isotherm represents the adsorbate in the liquid phase at the equilibrium concentration [53]. The isotherm study used to understand the extent and degree of favourability of adsorption. Experimental isotherm data can be fitted by several isotherm models such as Langmuir, Freundlich, and Dubinin-Radushkevitch isotherms.

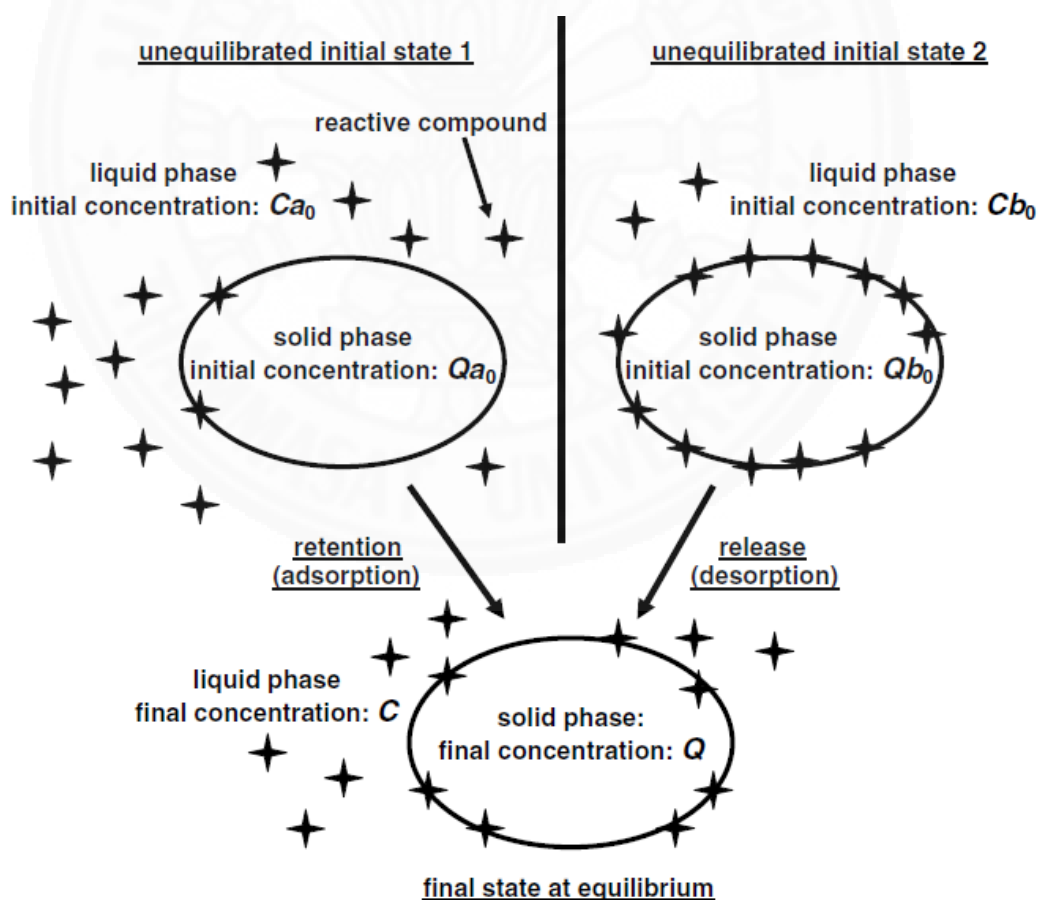


Figure 2.13 Phenomena of the adsorption and desorption [54]

### 2.3.1 Langmuir Isotherm

The Langmuir isotherm is the most popular isotherm which is two parameters. It refers to homogeneous and monolayer adsorption which explains the formation of adsorbate on surface of adsorbent in quantity. This model assumed that the molecules adsorbed on the surface and the neighboring adsorbed molecules do not interact [53]. The Langmuir model represents the relation between the equilibrium distribution of metal ions in the solid and liquid phases. In addition, this isotherm can be used to estimate the maximum adsorption capacity yielded when all sorption site are occupied. Two equivalent forms of the Langmuir isotherm, the linear and the non-linear, are given below: [55]

The linearized form

$$\frac{1}{q_e} = \left( \frac{1}{K_L q_m} \right) \frac{1}{C_e} + \frac{1}{q_m}$$

The non-linear form

$$q_e = \frac{q_m K_L C_e}{1 + K_L C_e}$$

Where:

$C_e$  = the equilibrium concentration of adsorbate (mg/L)

$q_e$  = the amount of metal adsorbed per gram of the adsorbent at equilibrium (mg/g)

$q_m$  = maximum monolayer coverage capacity (mg/g)

$K_L$  = Langmuir isotherm constant (L/mg)

The linear form plots between  $\frac{1}{q_e}$  and  $\frac{1}{C_e}$  while the graph of the non-linear form plots between  $q_e$  and  $C_e$ . Yuh-Shan Ho (2005) [56] suggested that the non-linear method is the better way to analyze the isotherm parameter because it has a higher coefficient of determination than linear equation.

Two parameters from the Langmuir isotherm can be obtained,  $q_m$  refers to the maximum adsorption capacity in unit of weight (mg of adsorbate per g of adsorbent) and  $K_L$  is the constant which is related to the adsorption free energy.

The essential parameters of the Langmuir isotherm called equilibrium parameters or separation factor which can be expressed in terms of a dimensionless constant as the following equation:

$$R_L = \frac{1}{1 + K_L C_0}$$

Where

$R_L$  = equilibrium parameter

$K_L$  = Langmuir isotherm constant (L/mg)

$C_0$  = the highest initial concentration (mg/L)

This parameter indicates the type of isotherm [53]. The values of  $R_L$  represents the condition of adsorption which are:  $R_L > 1$ ,  $R_L = 1$ ,  $0 < R_L < 1$ , and  $R_L = 0$  corresponding to unfavorable, linear, favorable, and irreversible type of adsorption, respectively [8].

### 2.3.2 Freundlich Isotherm

The Freundlich isotherm is the well-known relationship that used to describe the non-ideal and reversible adsorption. It can be applied to multilayer and heterogeneous adsorption which especially for highly interactive species on activated carbon and molecular sieves or organic compounds [57]. This model are also described in two forms following the equations:[56]

Linear form

$$\log(q_e) = \log(K_f) + \frac{1}{n} \log(C_e)$$

Non-linear form

$$q_e = K_f C_e^{1/n}$$

Where

$K_f$  = Freundlich isotherm constant (mg/g)

$n$  = adsorption intensity

$C_e$  = the equilibrium concentration of adsorbate (mg/L)

$q_e$  = the amount he amount of metal adsorbed per gram of the adsorbent at equilibrium (mg/g)

The graph of the linear form plots between  $\log q_e$  and  $\log C_e$  while the graph of non-linear plots between  $q_e$  and  $C_e$ . Two parameters were obtained of Freundlich isotherm by fitting the experimental data which are the  $K_f$  and  $1/n$ . The Freundlich constant,  $K_f$ , can be related to the adsorption capacity and the adsorption intensity of the adsorbent is  $n$ . A value of  $1/n$  indicate the type of isotherm to be irreversible ( $1/n = 0$ ), favorable ( $0 < 1/n < 1$ ), and unfavorable ( $1/n > 1$ ) [58].

### 2.3.3 Dubinin-Radushkevitch isotherm

The Dubinin-Radushkevitch isotherm (D-R) is also a two-parameter isotherm used for describing the liquid-solid adsorption [40]. The adsorbents in modern technology such as activated carbons, synthesis zeolites, porous solids, and inorganic gel use this isotherm to fit the experimental data. [59] Two forms of the D-R isotherm, the linear and the non-linear, are described by the following: [57]

Linear form

$$\ln(q_e) = \ln(q_s) - K_{DR}\varepsilon^2$$

Non-linear form

$$q_e = (q_s) \exp(-K_{DR}\varepsilon^2)$$

Where

$q_e$  =amount of adsorbate in the adsorbent at equilibrium (mg/g)

$q_s$  =theoretical isotherm saturation capacity (mg/g)

$K_{DR}$  =Dubinin–Radushkevich isotherm constant ( $\text{mol}^2/\text{kJ}^2$ )

$\varepsilon$  =Dubinin–Radushkevich isotherm constant calculate by

$$\varepsilon = RT \ln\left[1 + \frac{1}{C_e}\right]$$

Where

R =the gas constant (8.314 J/mol K)

T =absolute temperature (K)

$C_e$  =adsorbate equilibrium concentration (mg/L)

The linear form plots between  $\ln(q_e)$  vs  $\varepsilon^2$  while the non-linear form plots between the  $q_e$  versus  $C_e$ . The approach was normally applied to distinguish the chemical and physical adsorption of metal ions using the means adsorption free energy is  $E$  (kJ/mol) [57]. This value can be computed by the following

$$E = (2K_{DR})^{-1/2}$$

Where

E =the mean adsorption free energy (kJ/mol)

$K_{DR}$  =Dubinin–Radushkevich isotherm constant ( $\text{mol}^2/\text{kJ}^2$ )

The E values are between 1.0-8.0 kJ/mol for physical adsorption and 9.0-16.0 kJ/mol for chemical adsorption [60, 61].

## 2.4 Kinetic Study

The kinetic data important for analyzing the adsorption process because the kinetics can be used to explain the adsorbate uptake rate. Two widely used kinetic models are the pseudo-first-order and the pseudo-second-order models [62]. Lin, J. and L. Wang. (2009) suggest that the nonlinear forms are more suitable than the linear form for fitting the experimental data because the model parameters may possibly be distorted when the non-linear equations were transformed to linear forms [8, 63]. Thus, the non-linear method should be used to obtain the adsorption parameters.

### 2.4.1 Pseudo-First-Order Model

The pseudo-first-order is used to distinguish the kinetic equations based on adsorption capacity from solution concentration. It describes the kinetic process of liquid-solid phase adsorption which is believed to pertain the adsorption rate based on the adsorption capacity. In recent years, this model has been widely used to describe the adsorption of contaminant from wastewater [64]. The equation of pseudo-first-order in the linear and non-linear forms are as follows

Linear form

$$\ln(q_e - q_t) = \ln q_e - k_1 t$$

Non-linear form

$$q_t = q_e(1 - e^{-k_1 t})$$

Where

$q_t$  =the amount of adsorbate per unit mass of the adsorbent at any time (mg/g)

$q_e$  =the amount of adsorbed per unit mass of adsorbent at adsorption equilibrium (mg/g)

$k_1$  =pseudo-first-order constant ( $\text{min}^{-1}$ )

The graph of the linear form plots between  $\ln (q_{e,\text{exp}}-q_t)$  and  $t$  and the graph of the non-linear form plots between  $q_t$  and  $t$ .

#### 2.4.2 Pseudo-Second-Order Model

The pseudo-second-order model is used to describe a kinetic process of the adsorption of divalent metal ions in which the chemical bonding among divalent metal ion. The rate limiting step may be chemical adsorption involving valent forces through sharing or the exchange of electrons between the sorbents and divalent metal ions. It can be dominant in the adsorption of ions on sorbent, in addition, the adsorption follows the Langmuir equation [ 64 ]. This equation has been successfully applied to the metal ion adsorption such as dyes, herbicides, oils, and organic substances from aqueous solutions. The linear and non-linear forms of the pseudo-second-order model are given as:

Linear form

$$\frac{1}{q_t} = \frac{1}{q_e} + \frac{1}{k_2 q_e^2} \frac{1}{t}$$

Non-linear form

$$q_t = \frac{k_2 q_e^2 t}{1 + k_2 q_e t}$$

Where

$q_t$  =the amount of adsorbate per unit mass of adsorbent at any time (mg/g)

$q_e$  =the amount of adsorbate per unit mass of adsorbent at adsorption equilibrium (mg/g)

$k_2$  =pseudo-second-order constant ( $\text{g mg}^{-1} \text{min}^{-1}$ )

The values of  $\frac{1}{q_t}$  and  $\frac{1}{t}$  are plotted for the linear form and the values of  $q_t$  and  $t$  are plotted for non-linear form.

## Chapter 3

### Materials and methods

#### 3.1 Reagents

All chemical reagents used in this study were of analytical reagent grade (AR gr. For synthesis of adsorbents, titanium (IV) -isopropoxide (TiPO) 97% was purchased from Aldrich, tetraethylorthosilicate (TEOS) 98% was obtained from ACROS Organics and sodium hydroxide 98.1% was purchased from Fisher chemical. For stock solution preparation, lead nitrate ( $\text{Pb}(\text{NO}_3)_2$ ) was obtained from CARLO ERBA. LEWATIT<sup>®</sup> MonoPlus S 108 ion exchange resin was used to compare adsorption capacity.

#### 3.2 Instruments for Characterization

SEM images of all samples were taken by using JEOL Scanning Electron Microscope (SEM) JSM-5410LV and elemental composition was obtained by using Hitachi S-3000 SEM/EDX integrated analysis systems. The structural phase identification was determined using XRD PANalytical X' Pert PRO with Cu  $K\alpha$  radiation operating at 45kV and 45mA in two-theta degree mode. Scanning was performed from  $10^\circ$  to  $70^\circ$  with counting time of 0.5 s/step and a step size of 0.020. The structure was identified by comparison to patterns database in the JADE program.

Infrared spectra were recorded at room temperature using the attenuated total reflection mode ATR-FTIR (Thermo Scientific, iD spectrometer). The adsorbents were separated from aqueous solution by using centrifuge. The concentrations of metal solution were measured using PerkinElmer optima 8000 inductively coupled plasma-atomic emission spectroscopy (ICP-OES).

#### 3.3 Synthesis of Adsorbents

The conditions for synthesis of adsorbent can be classified into three methods. The various synthesis conditions and their codenames are listed below.

##### **SP-TSi-1h**

In this sorbent amorphous precursor (SP) was created by slowly reacting titanium (IV) isopropoxide (6.84g) with moisture at room temperature for 8 hours and become white slurry (**Figure 3.1**). The resulting white slurry was then mixed

with 5g of tetraethyl orthosilicate (TEOS). Then 23.68 g of NaOH in 123.1 ml of deionize water was added in to the mixture and continue stir ring for 1h at room temperature. The white powder product was washed several time s with deionize water and separated using centrifuge. The adsorbent was dry at 60°C overnight and kept in desiccator before use.

#### **SP-TSi-6hΔ**

This is the same as the SP-TSi-1h above but in this condition the mixture transferred to Teflon-line vessel which shows in **Figure 3.2** for hydrothermal treatment for 6h at 200C°. The product was washed several time s with deionize water and separated using centrifuge. Finally, the adsorbent was dry at 60°C overnight and kept in desiccator before use.

#### **LP-TSi-6hΔ**

Titanium (IV) isopropoxide ( 6.84 g ) was mixed with 5g TEOS in plastic beaker and transferred to Teflon-line vessel for hydrothermal treatment where 23.68 g of NaOH in 123.1 ml of DI water was added in to the mixture and heated up for 6h at 200C°. The product was washed several time s with deionize water and separated using centrifuge. Finally, the adsorbent was dry at 60°C overnight and kept in desiccator before use. Summary of the selected synthesis conditions are listed in the Table 3.1 below.

**Table 3.1 Synthesis conditions of adsorbents**

Name of adsorbents	Conditions					
	Liquid TiPO	Solid TiPO	TEOS	NaOH	Δ200°C 6h	Stir 1h
SP-TSi-1h	-	✓	✓	✓	-	✓
SP-TSi-6hΔ	-	✓	✓	✓	✓	-
LP-TSi-6hΔ	✓	-	✓	✓	✓	-





**Figure 3.1 Solid precursor**



**Figure 3.2 Hydrothermal reactor**

### **3.4 Lead Stock Solution**

The Pb (II) stock solution 6,000 mg/L was prepared by dissolving Pb (NO<sub>3</sub>)<sub>2</sub> 9.5913 g in 1000 ml of deionized water and diluted for the Pb (II) stock concentration range from 100 to 6,000 mg/L.

### **3.5 Adsorption Isotherm Study**

The adsorbents 10 mg were mixed with 5 ml of Pb (II) solution in different concentration (100, 1000, 2000, 4000 and 6000 mg/L) and placed on a rotary shaker at 200 rpm and room temperature. After 24 hours, the adsorbents were separated from the solution by centrifuge. Finally, the Pb (II) concentration after adsorption was measured using ICP-OES and each sample is repeated 3 times.

### **3.6 Kinetic Study**

The adsorbents 10 mg were mixed with 5 ml of Pb(II) solution 1,000 mg/L. The mixtures were placed on a rotary shaker at 200 rpm and room temperature in different times (0.25, 0.5, 1, 2, 4, 6, and 8 hours). Then the adsorbents were separated from the solution using centrifuge and the Pb(II) concentration after adsorption was measured by ICP-OES each sample is repeated 3 times

### **3.7 Regeneration**

The adsorbents after adsorption with initial concentration 1,000 mg/L were shaken with 4M NaOH, 1M HCL+4M NaOH, and 1M HCL at 200 rpm, varying time for 2, 4, and 24 h. The adsorbents were then washed with DI water 3 times and separated from DI water using centrifuge. The adsorbents were mixed again with Pb(II) solution 1000 mg/L and placed on a rotary shaker at 200 rpm, room temperature for 24 h. Finally, the adsorbents were separated from the solution by centrifuge and the Pb(II) concentration after reuse was measured by ICP-OES and each sample is repeated 5 times (5 cycles).

## Chapter 4

### Results and Discussions

#### 4.1 Synthesis of Adsorbent

**Figure 4.1 (a), (b), and (c)** illustrates the sorbents after drying which are SP-TSi-1h, SP-TSi-6h $\Delta$ , and LP-TSi-6h $\Delta$  respectively. The product of SP-TSi-1h without hydrothermal was washed several times with DI water and its last pH was 10. After dried overnight, it turned into a coarse-white powder. This is different from SP-TSi-6h $\Delta$  and LP-TSi-6h $\Delta$  which were synthesized under hydrothermal conditions at 200°C for six-hours. They were washed several times with DI water and their pH decreased to 7. After drying overnight, they turned into fine-white powder. The final product of LP-TSi-6h $\Delta$  is finer than SP-TSi-6h $\Delta$ .

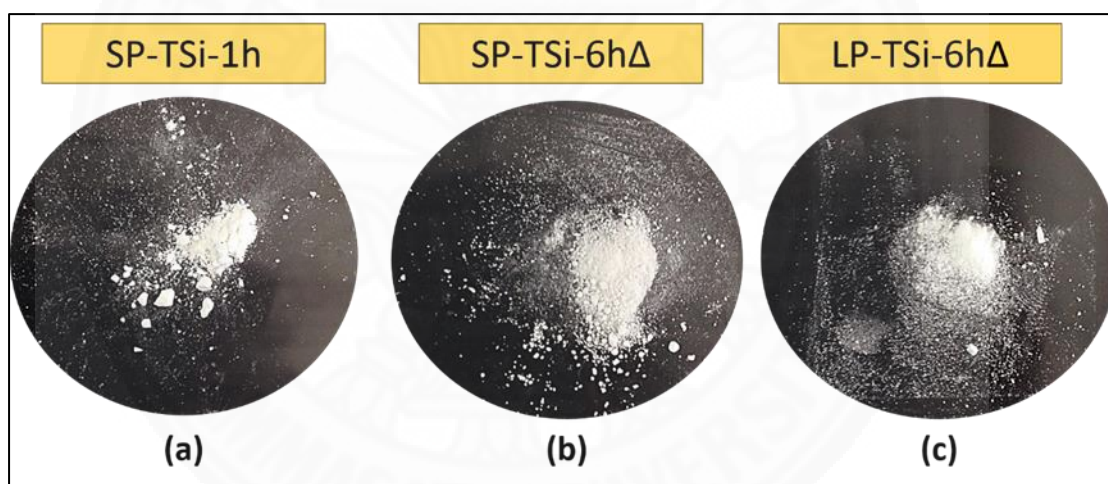


**Figure 4.1** Digital photograph of sorbents after drying of (a) SP-TSi-1h, (b) SP-TSi-6h $\Delta$ , and (c) LP-TSi-6h $\Delta$

#### 4.2 Preliminary Study

The preliminary test for the synthesized sorbent performance was conducted by using SP-TSi-6 $\Delta$  as adsorbent to adsorb Pb, Ni, Cr, and Cd. **Figure 4.2** shows that adsorbent named SP-TSi-6h $\Delta$  can adsorb Pb, Ni, Cr, and Cd are 401, 190.5, 2.5, and 1 mg/g, respectively. From the results, Pb shows the highest adsorption capacity. So Pb was selected to study in this work.

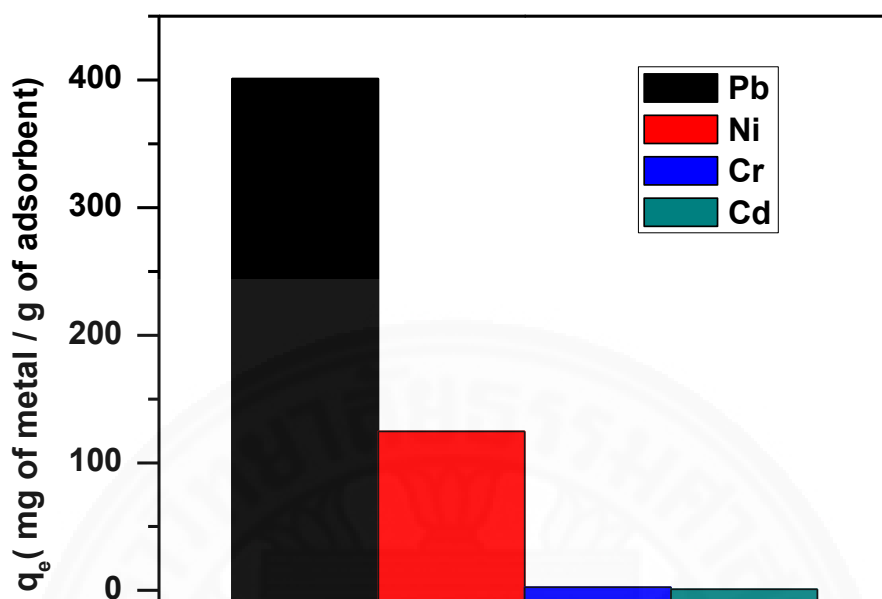


**Figure 4.2 Adsorption capacity,  $q_e$  (mg/g) of SP-TSi-6h $\Delta$  for preliminary study (initial concentration range: 1000 mg/L, metal solution volume 5 ml, adsorbent 10 mg, 200 rpm, room temperature, and 24h contact time)**

### 4.3 Characterization

#### 4.3.1 Scanning Electron Microscope (SEM)

The SEM images before adsorption of the fresh sorbents (before sorption experiment) SP-TSi-1h, SP-TSi-6h $\Delta$ , and LP-TSi-6h $\Delta$  are displayed in **Figure 4.3** (a), (b), and (c), respectively. It can be seen that for SP-TSi-1h sample which has not been subjected to any hydrothermal treatment, the sorbents have irregular shape with particle size ranges from a few to several tens of microns. Upon hydrothermal treatment for 6h at 200°C, the sorbent size starts to become smaller. This is probably due to the dissolution-recrystallization of the large-size sorbent in (a) forming smaller size particles with a rounder shape and uniform size distribution. When liquid precursor is employed in the hydrothermal synthesis as in LP-TSi-6h $\Delta$  (**Figure 4.3. (c)**), the sorbent obtained consists of small round-shape particles with quite a uniform size distribution

of about 4  $\mu\text{m}$ . When compared between before and after adsorption, the SEM images after adsorption of SP-TSi-TSi-1h, SP-TSi-6h $\Delta$  and LP-TSi-6h $\Delta$  are shown in **Figure 4.3** (d), (e) and (f) respectively.

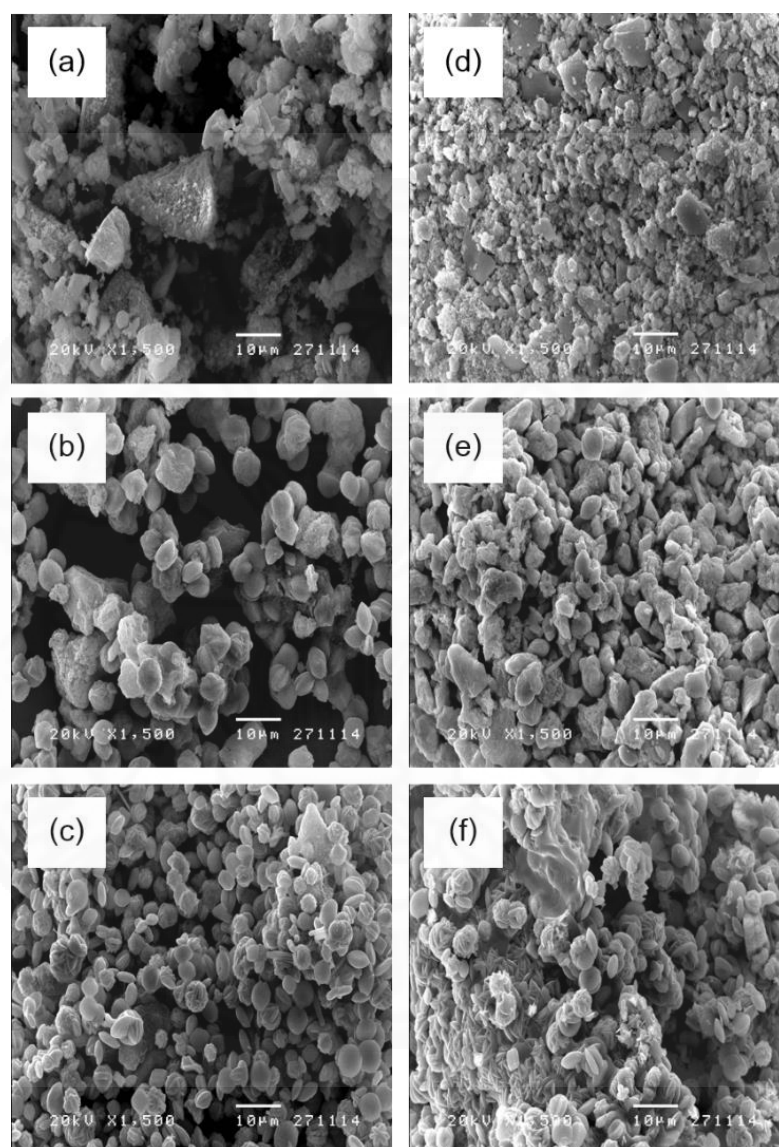


**Figure 4.3 SEM images: before adsorption of (a) SP-TSi-1h, (b) SP-TSi-6h $\Delta$ , and (c) LP-TSi-6h $\Delta$  and after adsorption of (d) SP-TSi-1h, (e) SP-TSi-6h $\Delta$ , and (f) LP-TSi-6h $\Delta$**

After Pb sorption, the SEM images of all the sorbents show that the sorbents have been corroded, the effect is more pronounced in the case of SP-TSi-1h (**Figure 4.3 a and d**), where large sorbent grain has been broken into smaller particles

indicating that the sorbents are brittle. For samples that have been under hydrothermal, the effect seems to be less pronounced with particles maintaining similar grain size. However, some surface corrosion can already be observed. The LP-TSi-6h  $\Delta$  (**Figure 4.3 c and f**) seems to be more resistance to corrosion than other structures.

#### 4.3.2 X-ray diffraction (XRD)

The patterns of XRD are illustrated in **Figure 4.4** which the sorbents of SP-TSi-1h, SP-TSi-6h $\Delta$ , and LP-TSi-6h $\Delta$  are (a), (b), and (c) respectively.

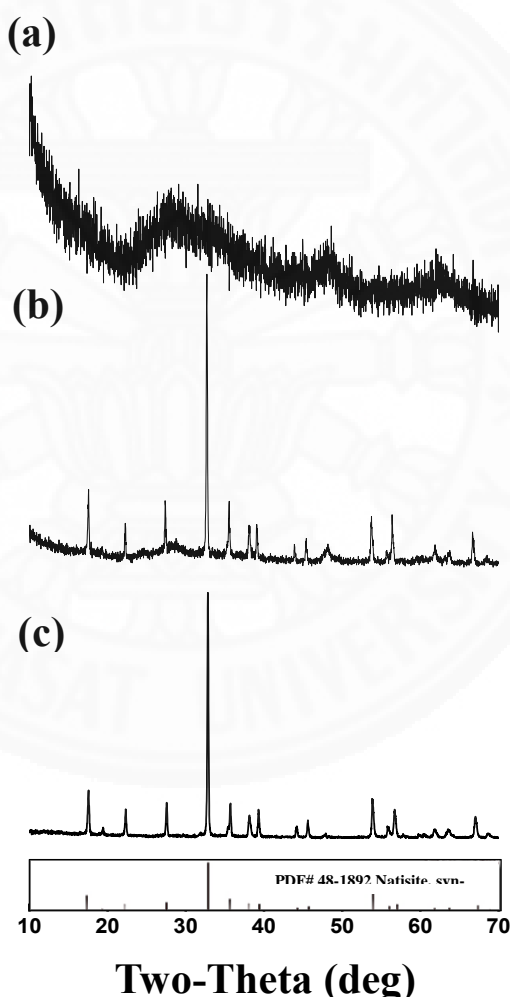


**Figure 4.4** XRD patterns before adsorption of (a) SP-TSi-1h, (b) SP-TSi-6h $\Delta$ , and (c) LP-TSi-6h $\Delta$

In the SP-TSi-1h, XRD pattern is typical of amorphous materials with some broad peaks around 30° and 50°. This is different from SP-TSi-6hΔ and LP-TSi-6hΔ which have been under hydrothermal treatment show several clear peaks at 17.55°, 32.75°, and 53.89° and other positions. These peaks can be matched with the reference XRD pattern of one of the titanosilicate compounds known as natisite ( $\text{Na}_2\text{TiOSiO}_4$ ) [9] Some amorphous phase still remains in the SP-TSi-6hΔ, indicating that the transformation and the growth of the natisite have not yet been completed.

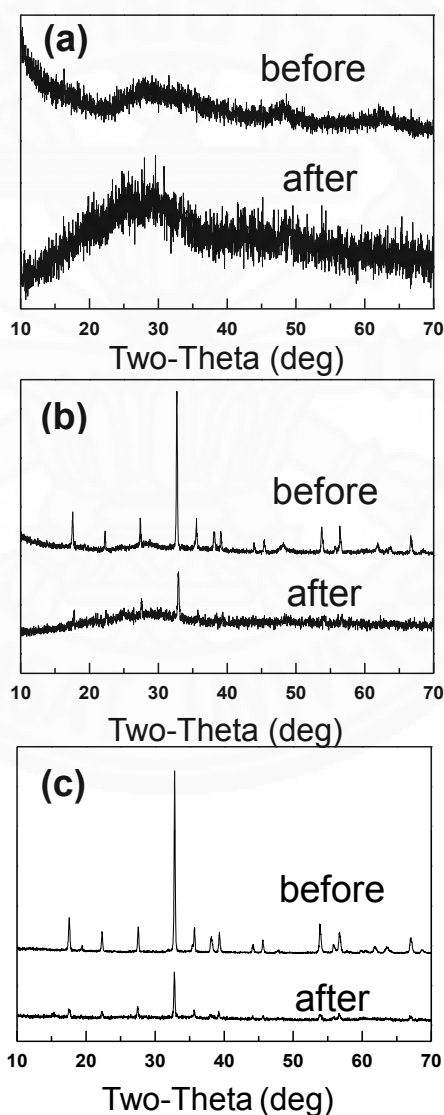


**Figure 4.5 XRD patterns compared between before and after adsorption of (a) SP-TEOS-1h, (b) SP-TSi-6hΔ, and (c) LP-TSi-6hΔ**

The diffractogram of **Figure 4.4** (C) is also sharper than sample (b), but the similar peak positions indicating that this is also natisite. The structures of (a), (b), and (c) are amorphous, semi-crystalline, and crystalline, respectively. The SEM image related to XRD pattern. The sorbent in without hydrothermal condition is unidentified the particle shape as amorphous. In the other hand, the particle shape of hydrothermal condition is uniform size clearly as crystalline. The comparison between before and after adsorption of XRD patterns are displayed in **Figure 4.5**. The XRD patterns of the adsorbents after Pb sorption shows significantly less amount of crystallinity than the pristine adsorbents. No new phase of Pb can be found in the XRD patterns of these samples after sorption.

#### 4.3.3 Fourier transform infrared (FT-IR)

**Figure 4.6** presents the FTIR spectrum comparison between before and after adsorption of SP-TSi-1h, SP-TSi-6h $\Delta$ , and LP-TSi-6h $\Delta$  are (a), (b), and (c) respectively. The absorption bands located at 616, 723, 839, and 881  $\text{cm}^{-1}$ . The peaks at 535-921  $\text{cm}^{-1}$  indicate the Ti-O bond. The results of FTIR correspond to that observe in the patterns of XRD and the images of SEM where the SP-TSi-1h shows amorphous. Sorbent SP-TSi-1h (a) is not seem to show any peaks. Similar to the SEM and XRD results which the particle size is irregular and the pattern is amorphous phase. While the sorbent SP-TSi-6h $\Delta$  and LP-TSi-6h $\Delta$  are form to be crystalline because of hydrothermal condition. After adsorption, spectral are tiny change similar to XRD patterns after adsorption which the peaks are decreased. However, the new peaks do not appear after adsorption. These results indicate that the functional groups on the surface of the sorbents did not affect the metal adsorption



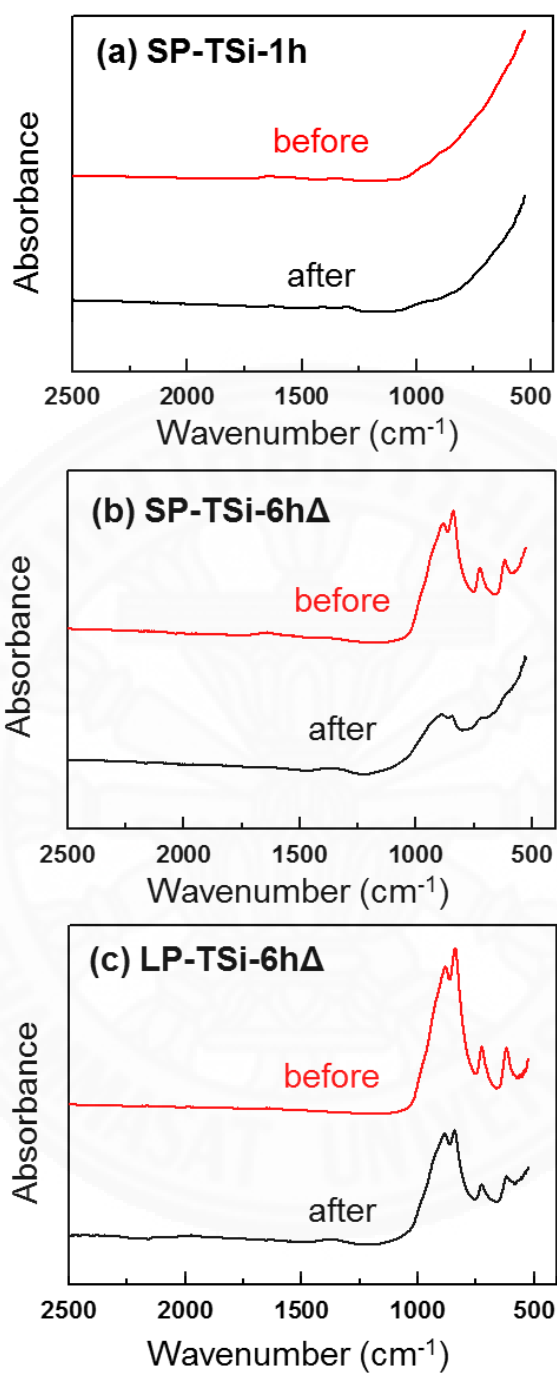


Figure 4.6 FTIR spectra before and after adsorption of (a) SP-TSi-1h, (b) SP-TSi-6h $\Delta$ , and (c) LP-TSi-6h $\Delta$

#### 4.3.4 Energy Dispersive X-ray spectrometer (EDS/EDX)

The Energy Dispersive X-ray spectrometer (EDS/EDX) results are shown in **Table 4.1**. These results show the different %amount of elements before and after adsorption. Percentages of Na decreased while percentages of Pb increased, after adsorption. The sorbents named SP-TSi-6h $\Delta$  and LP-TSi-6h $\Delta$  show a high percentage of Na. These adsorbents are synthesized by using hydrothermal synthesis and affect the adsorbent density. For this result the Na cannot be released to exchange with Pb. This is different from SP-TSi-1h which was stirred for 1h in which the percentage of Na before adsorption is lower but after adsorption it does not has the amount of Pb. Because the Na cannot form compound completely, Na can be released for exchange. This is the one results can be supported the mechanism and agree with ion-exchange results that have been reported later.

**Table 4.1 Chemical composition of adsorbents measured by The Energy Dispersive X-ray spectrometer (EDS/EDX)**

Name of adsorbent	Elements*	% by weight		Q <sub>max</sub> (mg/g)
		Before adsorption	After adsorption	
SP-TSi-1h	Na	5.78	0	473
	Si	1.21	1.20	
	Ti	46.91	35.27	
	Pb	0	37.49	
SP-TSi-6h $\Delta$	Na	14.64	0.76	453
	Si	13.41	6.10	
	Ti	28.99	37.32	
	Pb	0	23.70	
LP-TSi-6h $\Delta$	Na	14.57	11.50	405
	Si	11.52	13.53	
	Ti	21.20	27.05	
	Pb	0	2.64	

\* Major chosen elements

#### 4.4 Effect of Pb (II) Initial Concentration

The effect of initial Pb(II) concentration which ranges from 100-6000 mg/L on the adsorption capacity was investigated by shaking 10 mg of the adsorbent in 5 mL of Pb(II) solution for 24h at room temperature. The trend of changing Pb initial concentration on the adsorption capacity is illustrated in **Figure 4.7**. At relatively low concentration (100 mg/L), the adsorption capacity is lower than 100 mg/g. The adsorption capacity increase as the Pb concentration increase. When the initial concentration is higher than 1000 mg/L, the sorbents slow uptake. The possible reason may be too high solute concentrations, the adsorption process slow down [65].

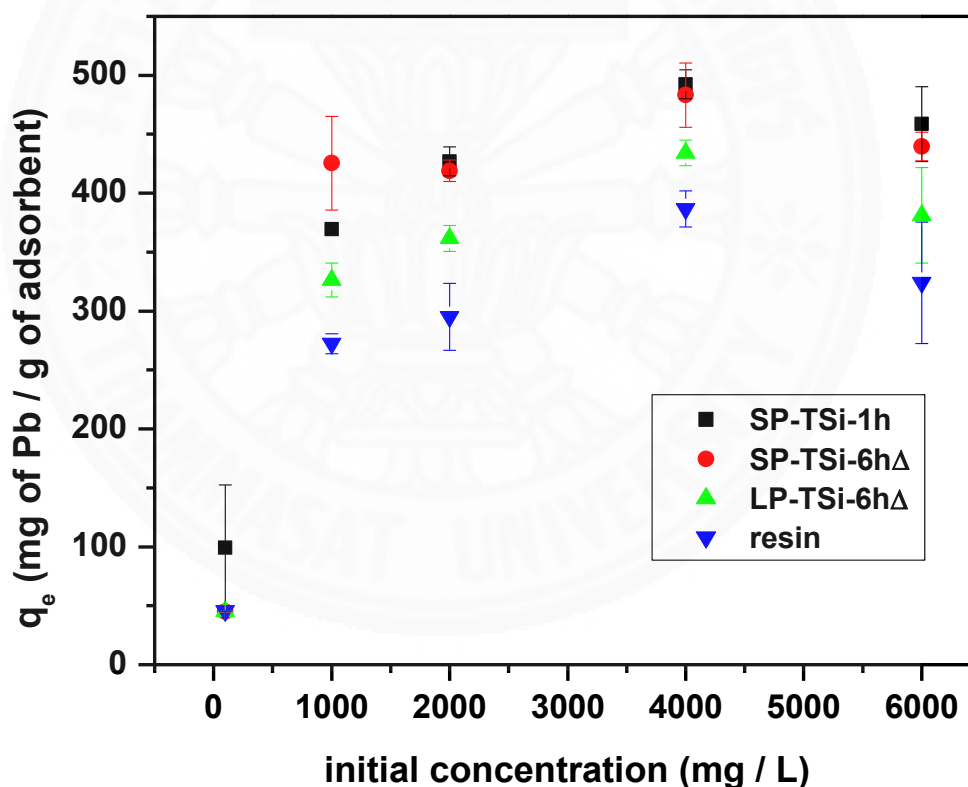


**Figure 4.7** Effect of initial concentration (mg/L) on Pb(II) adsorption capacity,  $q_e$  (mg/g) of SP-TSi-1h, SP-TSi-6hΔ, LP-TSi-6hΔ, and resin (initial concentration range: 100-6000 mg/L, Pb (II) solution volume 5 ml, adsorbent 10 mg, 200 rpm, room temperature, and 24h)

The final capacity at concentration of 6000 mg/L of the SP-TSi-1h, SP-TSi-6hΔ, LP-TSi-6hΔ, and resin are 459, 440, 381, and 324 mg/L, respectively. The sorbent named SP-TSi-1h which has the highest amorphous phase and without hydrothermal condition has the highest capacity.

#### 4.5 Effect of contact time

The effect of the contact time on the Pb removal is shown in **Figure 4.8**. It can be seen that the concentration of Pb in the solution decreases rapidly within the first hour of contact time, and reaches fairly constant level after about 1 hours of contact time with the adsorbents. When the 8 hours were passed, the highest final capacity of SP-TSi-1h, SP-TSi-6hΔ, LP-TSi-6hΔ, and resin are 232, 235, 234, and 232 mg/L, respectively.

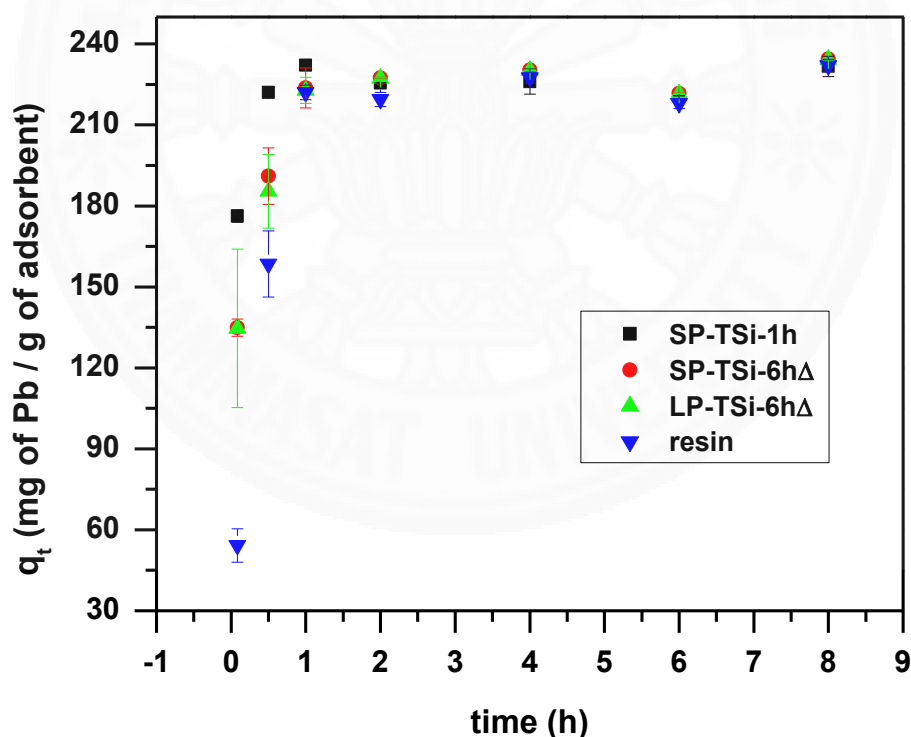


**Figure 4.8 Effect of contact time (5 min-8h) on Pb (II) adsorption capacity,  $q_t$  (mg/g) (Initial concentration 1000 mg/L, solution volume 5 ml, adsorbent 10 mg, 200 rpm at room temperature)**

## 4.6 Adsorption Isotherm

The adsorption isotherms were constructed by varying the initial concentration of Pb (II) from 100-6000 mg/L with constant sorbent titanosilicate 2g/L at room temperature and shaken at 200 rpm. The relationship between the amount of ions adsorbed by unit mass of the adsorbent and the ions remaining concentration in solution at equilibrium represented sorption isotherm. Adsorption isotherms were analyzed in the form of nonlinear models, using the Origin software to fit the data curves.

### 4.6.1 Langmuir isotherm

Langmuir isotherm describe the equilibrium experimental data. This model assumes that the adsorbent is homogeneous and the adsorption processes is monolayer. The equation of Langmuir model is given by: [55]

$$q_e = \frac{q_m K_L C_e}{1 + K_L C_e}$$

Where  $q_e$  = equilibrium sorption capacity (mg/g)

$q_m$  = maximum adsorption capacity (mg/g)

$K_L$  = the Langmuir constant for the affinity of Pb(II) ions onto the adsorbents

$C_e$  = equilibrium concentration of adsorbate in solution (mg/L)

The plot of  $q_e$  (mg/g) versus  $C_e$  is displayed in **Figure 4.9**.

### 4.6.2 Freundlich isotherm

Freundlich isotherm based on the heterogeneous surface and multilayer adsorption. [8] The Freundlich isotherm in nonlinear form can be written as: [56]

$$q_e = K_F C_e^{\frac{1}{n}}$$

where  $q_e$  = equilibrium sorption capacity (mg/g)

$C_e$  = concentration in equilibrium (mg/L),

$K_F$  = constant (L/g)

The plot of  $q_e$  (mg/g) versus  $C_e$  is shown in **Figure 4.10**.

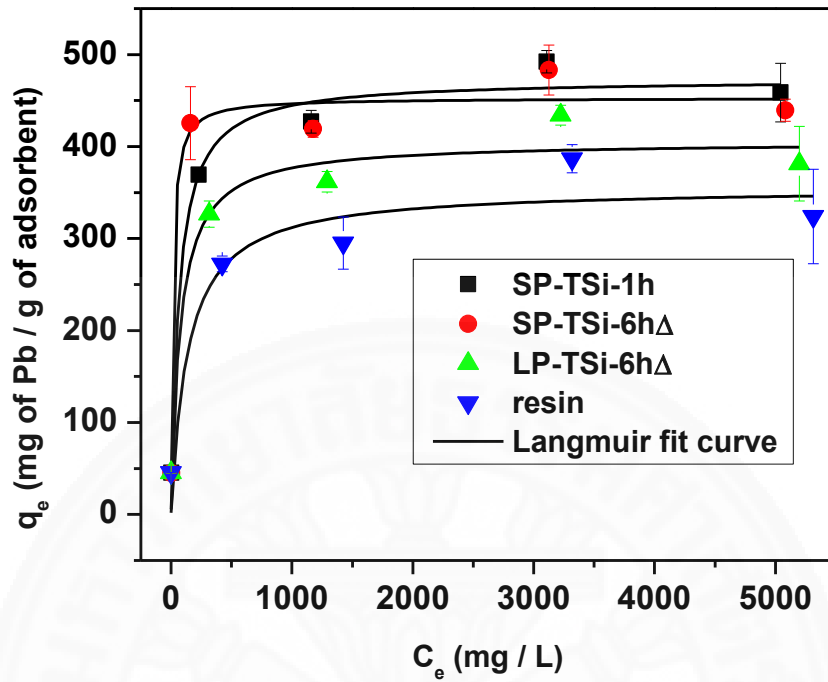


Figure 4.9 Adsorption isotherm of Pb(II) adsorption onto the four adsorbents together with the fit to the Langmuir isotherm model

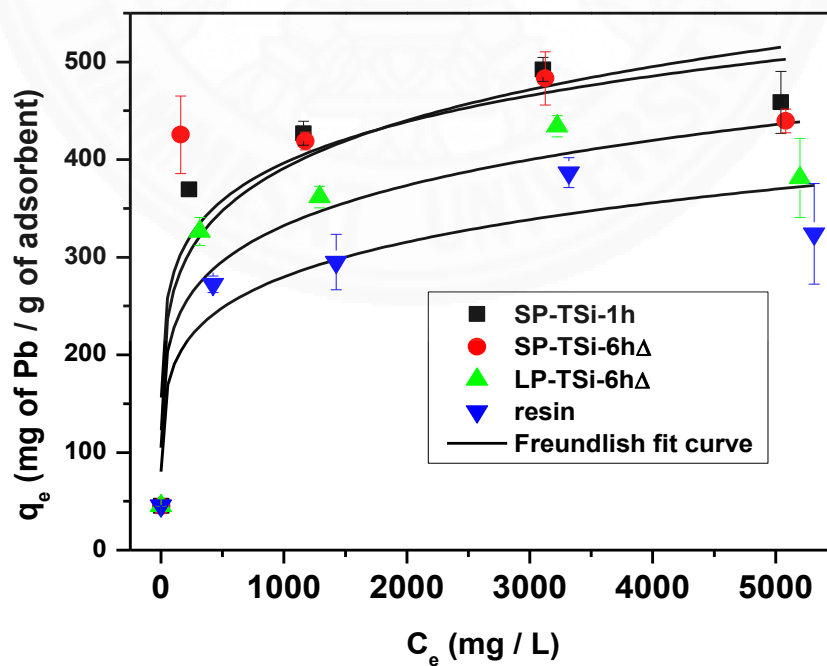


Figure 4.10 Adsorption isotherm of Pb(II) adsorption onto the four adsorbents together with the fit to the Freundlich isotherm model

#### 4.6.3 Dubinin-Radushkevich isotherm (D-R)

Dubinin–Radushkevich isotherm which is an obvious model applied to express the adsorption mechanism with a Gaussian energy distribution onto a heterogeneous surface. The equation in nonlinear form is followed by: [57]

$$q_e = (q_s) \exp(-K_{DR}\epsilon^2)$$

Where  $q_e$  =amount of adsorbate in the adsorbent at equilibrium (mg/g)

$q_s$  =theoretical isotherm saturation capacity (mg/g)

$K_{DR}$ =D-R isotherm constant ( $\text{mol}^2/\text{kJ}^2$ )

$\epsilon$ =D-R isotherm constant

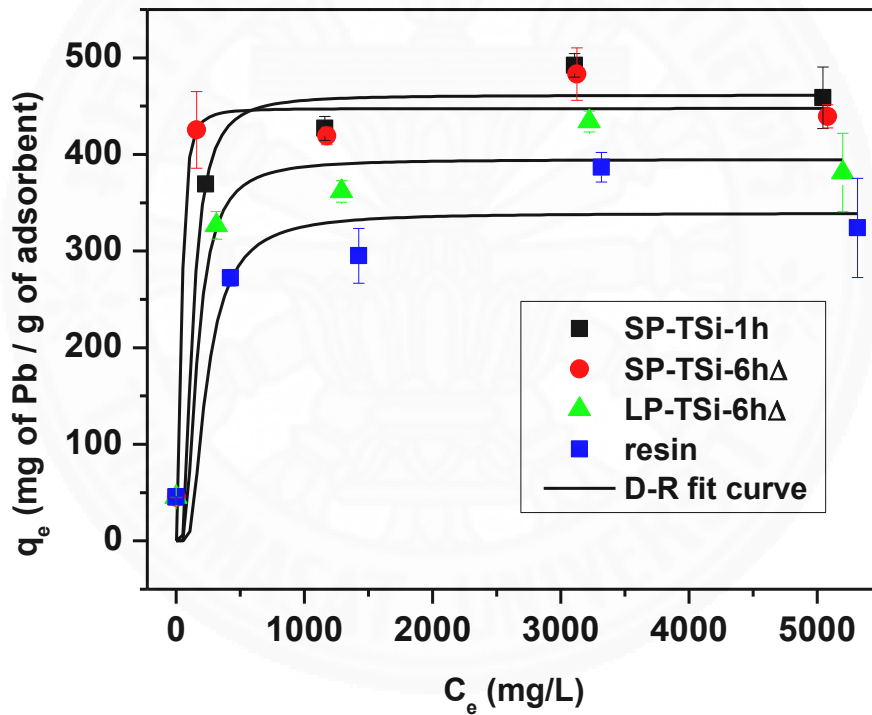


Figure 4.11 Adsorption isotherm of Pb(II) adsorption onto the four adsorbents together with the fit to the Dubinin-Radushkevich isotherm model

All the equations used Origin 7.0 software to fit the graphs. As seen in **Table 4.2**, the related parameters were calculated by the Langmuir, Freundlich, and D-R equations. The curves show a similar trend. The Pb(II) adsorption increases sharply at low equilibrium concentration, and starts to levels off. The maximum adsorption capacity ( $q_{\max}$ ) which fits by the Langmuir isotherm model of SP-TSi-1h, SP-TSi-6h $\Delta$ , LP-TSi-6h $\Delta$ , and resin are 473, 453, 405, and 355 mg/g, respectively.

For the equilibrium parameter ( $R_L$ ) can be computed by

$$R_L = \frac{1}{1 + K_L C_0}$$

Where

$R_L$  =equilibrium parameter

$K_L$  =Langmuir isotherm constant (L/mg)

$C_0$  =the highest initial concentration (mg/L)

The low  $R_L$  values of all adsorbents are in the range  $0 < R_L < 1$  (0.0023-0.0226). This result indicates that the titanosilicate sorbents was high favorable for the lead removal from aqueous solution [53].

For the Freundlich isotherm, the adsorption capacity ( $K_f$ ) of SP-TSi-1h, SP-TSi-6h $\Delta$ , LP-TSi-6h $\Delta$ , and resin are 121, 145, 104, and 85 mg/g, respectively. The Freundlich parameter, the adsorption intensity of the adsorbent ( $n$ ), the values are less than unity and more than zero (0.1462-0.1733). This result proves that the adsorption process is favorable and agree with  $R_L$  of Langmuir isotherm.

The curves were fit by the D-R isotherm model. The maximum adsorption capacity of SP-TSi-1h, SP-TSi-6h $\Delta$ , LP-TSi-6h $\Delta$ , and resin are 461, 442, 437, and 339 mg/g, respectively. For investigate the type of adsorption process which are physical and chemical adsorption are used the equation follow as:

$$E = (2K_{DR})^{-1/2}$$

Where

$E$  =the means adsorption free energy (kJ/mol)

$K_{DR}$  =Dubinin–Radushkevich isotherm constant ( $\text{mol}^2/\text{kJ}^2$ )



The calculation of E value shows in the range of 8.64-48.51 kJ/mol indicating the chemical adsorption. Especially, SP-TSi-6hΔ is the high E value that can be referred to the strong chemical adsorption.

The  $R^2$  values which obtain by fitting the above three models for presenting the experimental data followed the order: Langmuir > D-R > Freundlich. The high values of  $R^2$  for SP-TSi-1h (0.972), SP-TSi-6hΔ (0.978), LP-TSi-6hΔ (0.946), and resin (0.895) supported which these adsorption behaviour followed the Langmuir isotherm. When compared to resin which is the adsorbents for the household strainer, the titanosilicate sorbents are higher.

The titanosilicate sorbents are followed by the Langmuir isotherm which is the monolayer adsorption. Although the concentration of Pb(II) is increased, the adsorption capacity is stable. The adsorbents cannot adsorb the lead ions anymore. Normally, the chemical adsorption usually occurs in the monolayer adsorption with the high energy interaction and involve the exchange of ions.

**Table 4.2 Summary isotherm parameters for the adsorption of lead (II)**

Isotherm	parameters	Name of adsorbents			
		SP-TSi-1h	SP-TSi-6hΔ	LP-TSi-6hΔ	resin
Langmuir Isotherm	$q_{\max}$ (mg/g)	473.2	452.8	405.2	355.2
	$K_L$ (L/mg)	0.0155	0.0715	0.0132	0.0072
	$R^2$	0.972	0.978	0.946	0.895
	$R_L$	0.0106	0.0023	0.0125	0.0226
Freundlich Isotherm	$K_f$ (mg/g)	120.7	144.5	103.9	84.6
	1/n	0.1702	0.1462	0.1683	0.1733
	$R^2$	0.853	0.670	0.847	0.873
Dubinin-Radushkevich	$q_s$ (mg/g)	461.4	447.5	394.8	339.2
	$K_{DR}$ (mol <sup>2</sup> /kJ <sup>2</sup> )	0.0019	2.125E-04	0.0031	0.0067
	$R^2$	0.959	0.957	0.933	0.880
	E (kJ/mol)	16.22	48.51	12.70	8.64

#### 4.7 Kinetic Study

The adsorption kinetics have been experimented with two commonly employed kinetics models which is the pseudo-first-order [62] and the pseudo-second-order model [62]. The adsorption capacity at time t ( $q_t$ ) of all sorbents are plotted against time (min) and fitted by the equation of each model via Origin 7.0 software.

#### 4.7.1 Pseudo-first-order model

$$q_t = q_e[1 - \exp(-k_1 t)]$$

Where  $k_1$  = the first-order adsorption rate constants ( $\text{min}^{-1}$ )

$q_e$  = the equilibrium adsorption capacity ( $\text{mg/g}$ )

$q_t$  = the adsorption capacity at time  $t$  ( $\text{mg/g}$ )

The graphs of Pseudo-first-order are displayed in **Figure 4.12**.

#### 4.7.2 Pseudo-second-order model

$$q_t = \frac{k_2 q_e^2 t}{1 + k_2 q_e t}$$

Where  $k_2$  = the pseudo-second order adsorption rate constant ( $\text{g mg}^{-1} \text{min}^{-1}$ )  $q_e$  = the equilibrium adsorption capacity ( $\text{mg/g}$ )

$q_t$  = the adsorption capacity at time  $t$  ( $\text{mg/g}$ ).

**Figure 4.13** is shown the plots of Pseudo-second-order model.

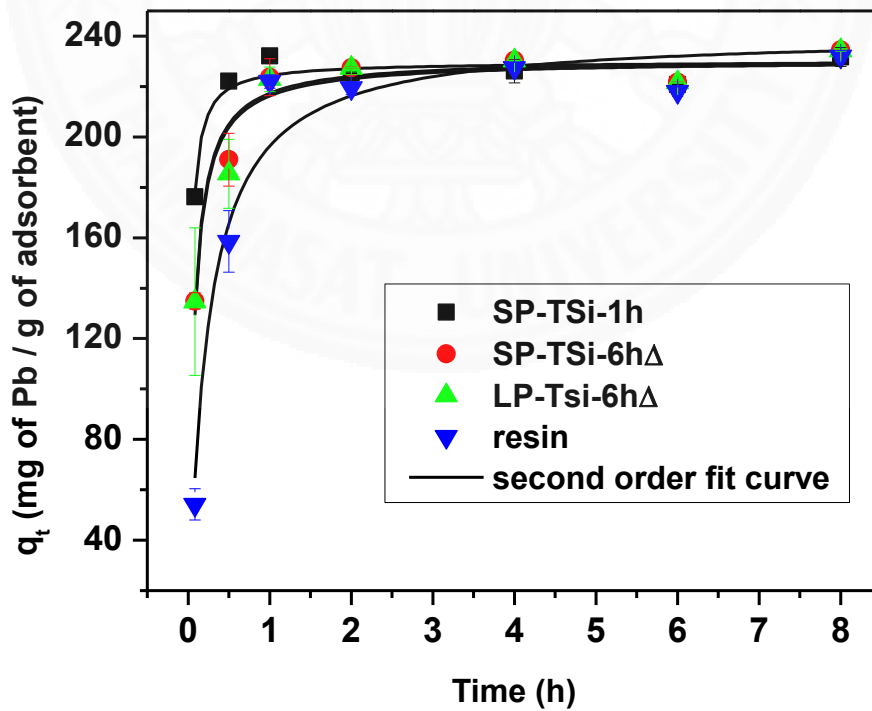


**Figure 4.12** Pseudo-first-order kinetic model for the adsorption of Pb(II) onto the synthesized adsorbent

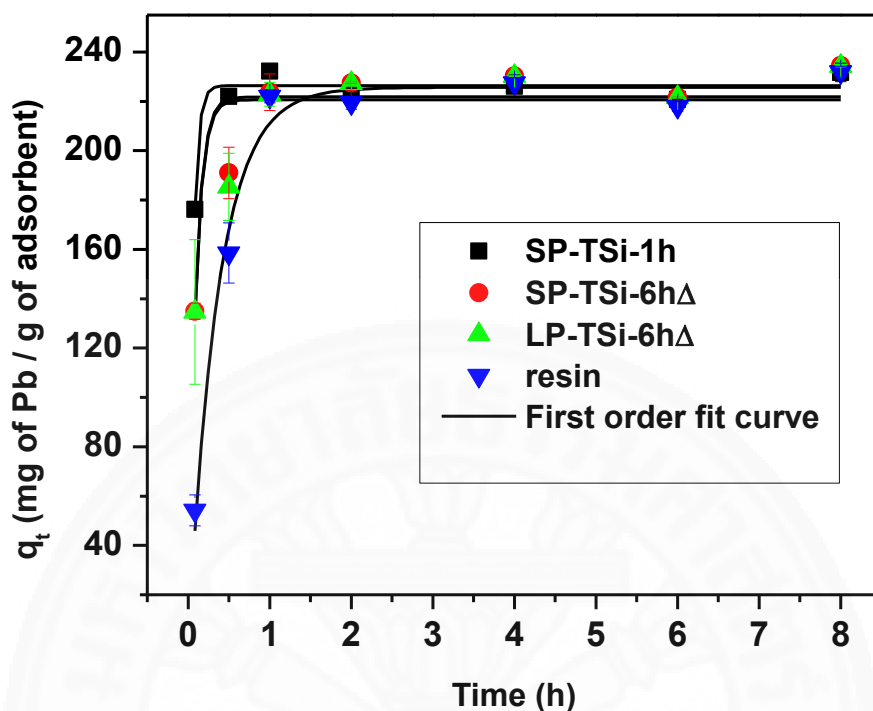


**Figure 4.13 Pseudo-second-order kinetic model for the adsorption of Pb(II) onto the synthesized adsorbents**

From two kinetic models, it can be clearly indicated that all the titanosilicate adsorbents have a fast kinetics initially, and the adsorption rate gradually slows down until it reaches the adsorption equilibrium within 1 h. It shows that the adsorption sites are available at the initial stage due to the large surface area of the adsorbent available for sorption. Then adsorbate formed a thick layer and the adsorption sites are gradually occupied with the adsorption process until all of them are not be free.

The values of kinetic parameters accomplished from the fitting are displayed in **Table 4.3**. It can be observed that the  $R^2$  values of the pseudo-first order model are range between 0.769 - 0.980. The pseudo-second order model shows the  $R^2$  values 0.919-0.951. In term of  $R^2$  values, SP-TSi-1h and resin well fit to the pseudo-first-order model while SP-TSi-6hΔ and LP-TSi-6hΔ agree with the pseudo-second order model. The samples were well fit to the pseudo-second order model, SP-TSi-6hΔ and LP-TSi-6hΔ, indicating the adsorption process is chemical adsorption.

**Table 4.3 Summary kinetic parameters for the adsorption of lead (II)**

Name of adsorbent	Pseudo-first order			Pseudo-second order		
	$q_e$ (mg/g)	$K_1$ (1/m)	$R^2$	$q_e$ (mg/g)	$K_2$ (g mg <sup>-1</sup> min <sup>-1</sup> )	$R^2$
SP-TSi-1h	226.40	7.851	0.940	229.83	0.178	0.919
SP- TSi -6hΔ	221.81	4.775	0.817	231.15	0.068	0.945
LP- TSi -6hΔ	220.66	4.786	0.769	230.37	0.066	0.921
Rein	225.69	1.186	0.980	240.83	0.018	0.951

#### 4.8 Ion-Exchange

The mechanism of Pb(II) sorption onto our zeolitic-like sodium titanosilicate may be due to several mechanisms such as adsorption of Pb(II) onto the pore structure as well as the ion-exchange of the Pb(II) with the Na<sup>+</sup> in the sorbent. For the ion-exchange mechanism, it is expected that two sodium ions should be released for the adsorption of one Pb(II). In this study, the ranges of Pb(II) initial concentration are varied between 100-6000 mg/L. The concentration of sodium released and lead adsorbed were measured and listed in **Table 4.4**. Normally, one bivalent cation can exchange two monovalent ions[66]. In this process, at the low initial concentration (100 mg/L) the mole ratio between Pb(II) and Na<sup>+</sup> ions is more than 2. Because the adsorbents are base which has a lot of Na<sup>+</sup> but the amount of Pb<sup>2+</sup> are not enough to exchange with Na<sup>+</sup>. In addition, they are very close to 2 when the initial concentration is more than 1000 mg/L. The results indicate that ion-exchange between the Pb<sup>2+</sup> and the Na<sup>+</sup> is the dominant mechanism for lead sorption here. The ratio between the Na<sup>+</sup> released to the Pb<sup>2+</sup> adsorbed is less than 2 indicates that some of the Pb<sup>2+</sup> may have been adsorbed without the exchange of Na<sup>+</sup> from the sorbent. This indicates that other Pb<sup>2+</sup> adsorption mechanisms may also be operating such as physical adsorption as well as chemical precipitation of the Pb<sup>2+</sup> onto the sorbent surface.

**Table 4.4 Ratio of mole Na<sup>+</sup> /mole Pb<sup>2+</sup> by vary the Pb(II) initial concentration (adsorbent dose of 2g/L, room temperature, 200 rpm for 24h)**

Initial concentration (mg/L)	mole Na <sup>+</sup> /mole Pb <sup>2+</sup>			
	SP-TSi-1h	SP-TSi-6hΔ	LP-TSi-6hΔ	resin
100	4.51	5.00	3.86	2.46
1000	1.89	1.93	1.87	1.97
2000	1.68	1.88	1.80	1.85
4000	1.38	1.59	1.49	1.46
6000	1.89	1.75	1.71	1.79

#### 4.9 Regeneration

Experiments were carried out using a commonly utilized method which is multiple adsorptions/desorption cycles. Firstly, the acid and base chemicals were used to regenerate the adsorbents which are 4M NaOH and 1M HCL. The regenerated conditions are obtained by shaking the adsorbent after adsorption with 4M NaOH for 24h, 1M HCL for 4h followed by 4M NaOH for 24 h, and 1M HCL for 24h. The adsorption capacity after regenerate and treat with the 1,000 mg/L of Pb(II) solution is shown in **Figure 4.14**. The results show that the best condition for regeneration is 4M NaOH. This is due probably to the Na is the major element of titanosilicate structures. When Na were treated again resulting the amount of Na in the structure increased and can be exchange with the Pb ions. Secondly, the adsorbent named SP-TSi-6hΔ which were regenerated by using 4M NaOH, the times have been varied for 2, 4, and 24h, as display in **Figure 4.15**. For 2h is suitable contact time which shows the highest adsorption capacity.

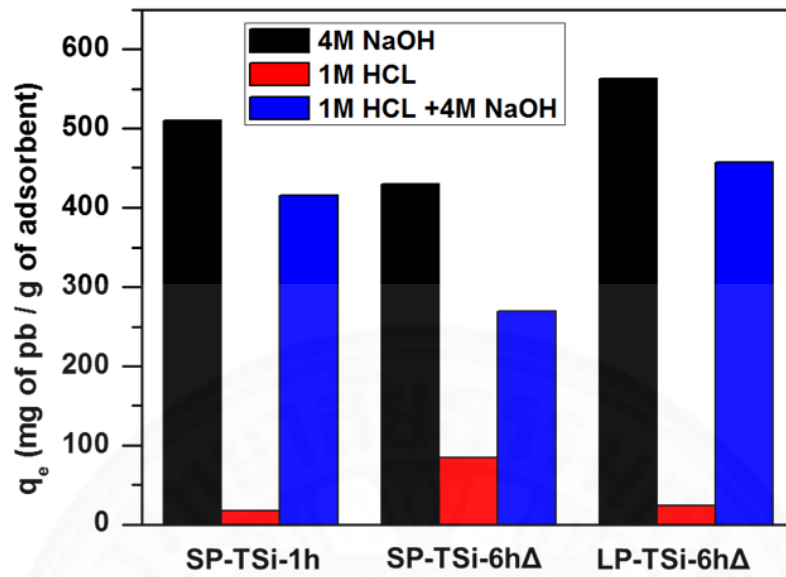


Figure 4.14 Adsorption capacity,  $q_e$  (mg/g) of SP-TSi-1h, SP-TSi-6h $\Delta$ , and LP-TSi-6h $\Delta$  after regeneration on various conditions

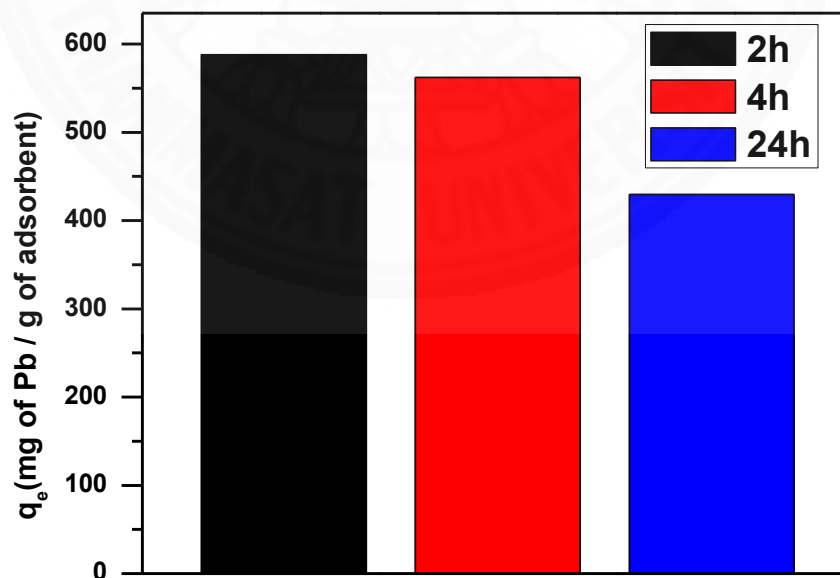
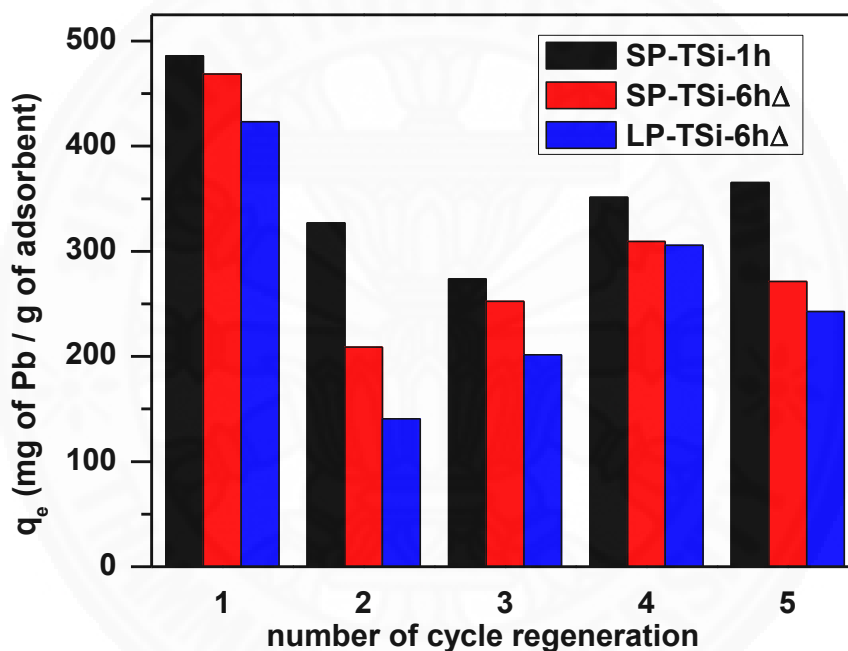


Figure 4.15 Adsorption capacity,  $q_e$  (mg/g) of SP-TSi-6h $\Delta$  after regenerated by 4M NaOH for 2, 4, and 24h

The titanosilicate sorbents were regenerated for five cycle. The Pb(II) adsorption results after each regeneration are shown in **Figure 4.16** For the SP-TSi-1h sorbent, the adsorption capacity of each cycle 1<sup>st</sup>, 2<sup>nd</sup>, 3<sup>rd</sup>, 4<sup>th</sup>, and 5<sup>th</sup> are 486, 327, 274, 351, and 365, respectively. For the SP-TSi-6hΔ sorbent, the adsorption capacity for the cycle of 1<sup>st</sup>, 2<sup>nd</sup>, 3<sup>rd</sup>, 4<sup>th</sup>, and 5<sup>th</sup> are 469, 208, 253, 309, and 203, respectively. For the LP-TSi-6hΔ sorbent, the adsorption capacity of the 1<sup>st</sup>, 2<sup>nd</sup>, 3<sup>rd</sup>, 4<sup>th</sup>, and 5<sup>th</sup> cycle are 423, 141, 202, 306, and 243, respectively.



**Figure 4.16** Adsorption capacity at equilibriums,  $q_e$  (mg/g) after the number of regeneration cycles

According to the chart in **Figure 4.16**, the adsorption capacity increases in the third cycle probably due to the release of remaining Na [41]. After that, the structures were deteriorated because of the continuous regeneration [41]. The adsorption capacity in the last cycle is lower than the first time 20-50%. However, the experiments show the promising possibility of the sorbent regeneration. Hence, titanosilicate sorbent can be used at least 5 times for Pb(II) removal. Fourier transform infrared (FT-IR)

spectrometer was used to analyze to compare the sorbent structures between after adsorption and after reuse for five times which are shown in **Figure 4.17**.

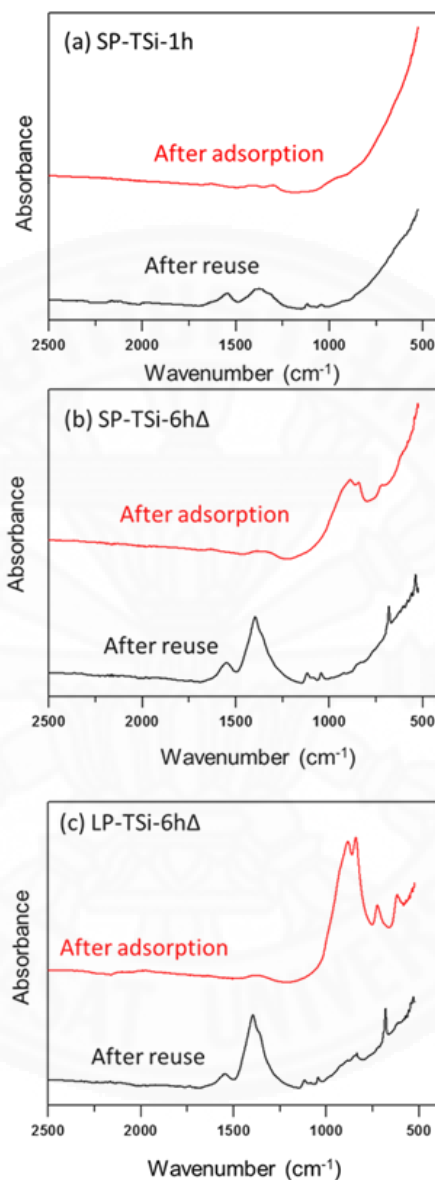


**Figure 4.17** FTIR spectra compare between after adsorption and after reuse of SP-TSi-1h, SP-TSi-6hΔ, and LP-TSi-6hΔ



The structures after reuse are changed when compare after adsorption. The new peak is sharp at  $1352\text{ cm}^{-1}$ . For this results, we assumed that the  $\text{Pb}(\text{OH})_2$  spectra will show in the structure probably caused Pb will be precipitated by concentrated base solution and transform to  $\text{Pb}(\text{OH})_2$  compound. For preparing the  $\text{Pb}(\text{OH})_2$ , the 4M NaOH was added in the Pb(II) solution with the initial concentration 6,000 mg/L. After that, the mixture was washed several times with DI water and separated by centrifuge.

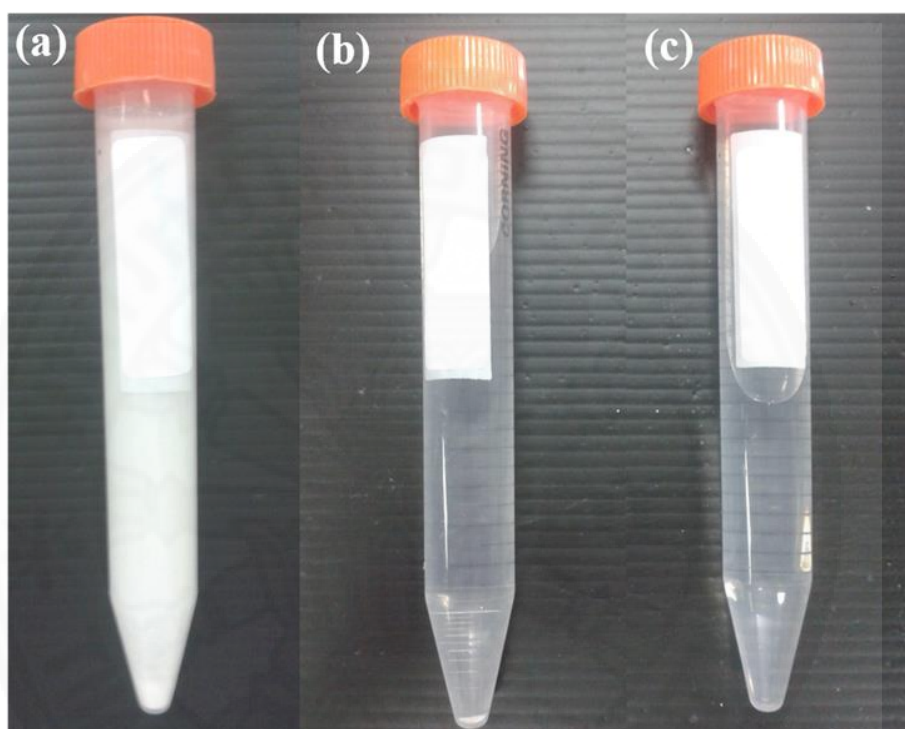


**Figure 4.18**  $\text{Pb}(\text{OH})_2$  preparation (a) added by 5M NaOH, (b) after centrifuge, and (c) DI water

**Figure 4.18** shows the  $\text{Pb}(\text{OH})_2$  preparation. NaOH was dropped in to the Pb(II) solution and the white suspensions occur in the liquid (a). After centrifuge, the solid phase is separated from the liquid phase and precipitate at the bottom (b). The solution is clear similar to DI water (C). The solid phase was dried at  $60\text{ }^\circ\text{C}$  overnight and turn into white powder. The spectra that adsorb from the  $\text{Pb}(\text{OH})_2$  powder are illustrated in **Figure 4.19**.

There are six major bands for characterization of  $\text{Pb}(\text{OH})_2$ . The strong bands are observed at about 680, 841, and  $1352\text{ cm}^{-1}$ . Others weak peaks appeared at 968, 1044, and  $1113\text{ cm}^{-1}$ . After five cycles of regeneration, the sorbents are characterized by FTIR and the similar peak positions to those of the  $\text{Pb}(\text{OH})_2$  occurred after regeneration. Because the sorbents were regenerated by concentrated base solution (5M NaOH) and the Pb ions may be precipitated into the hydroxide compound. The FTIR spectra of  $\text{Pb}(\text{OH})_2$  compared with the spectra of the sorbents after reuse are shown in **Figure 4.20**.

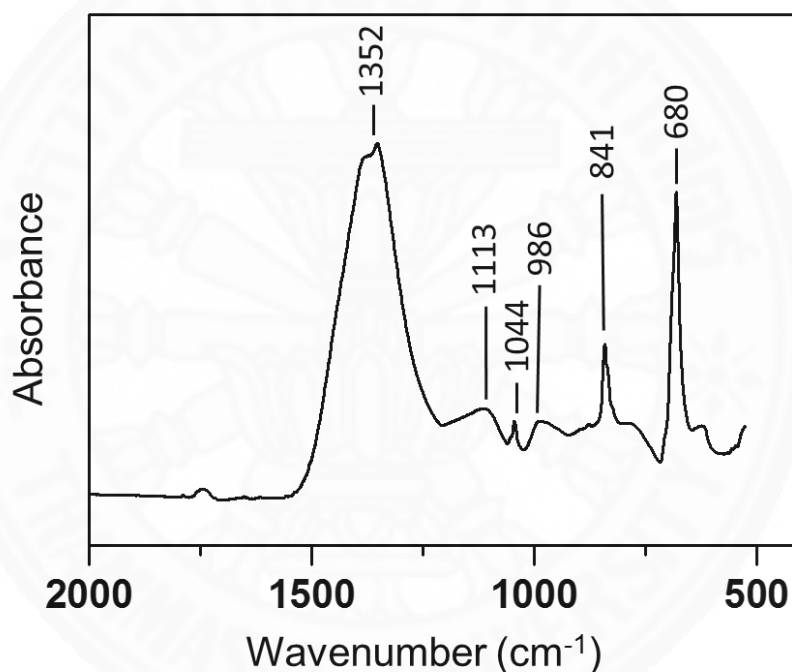


**Figure 4.19** FTIR spectra of  $\text{Pb}(\text{OH})_2$

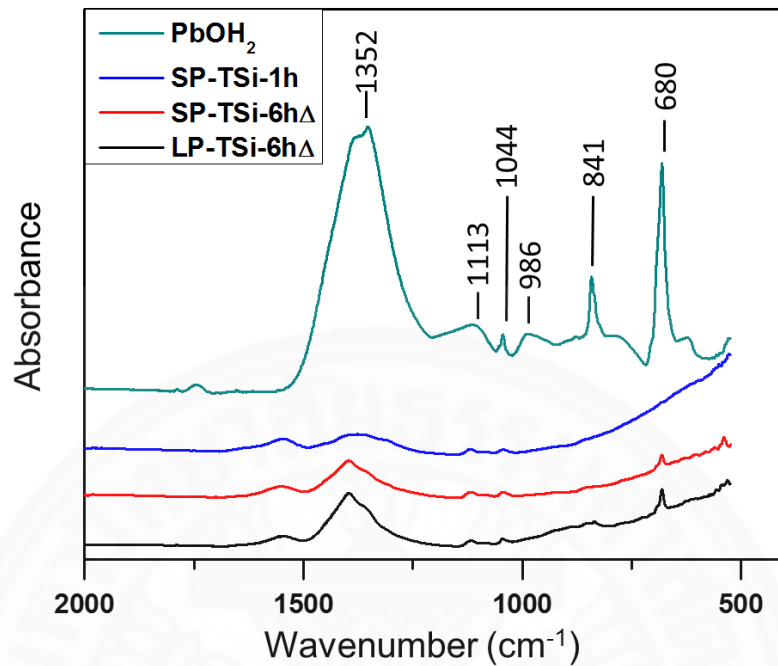


**Figure 4.20 FTIR spectra compare between Pb(OH)<sub>2</sub> and the adsorbents after reuse**

The results found that the adsorbents after reuse show peaks in the same position as that of Pb(OH)<sub>2</sub>. The adsorbents after regeneration has a high amount of Na because they are regenerated by NaOH and become the highly alkaline adsorbents. When Pb(II) solution were treated again, Pb ions reacted with OH and precipitate to be Pb(OH)<sub>2</sub>. So the structure of regenerated adsorbents appeared to have peaks of the Pb(OH)<sub>2</sub>.

## Chapter 5

### Conclusions

Sorbents based on sodium titanosilicates were successfully synthesized using different precursors and under different hydrothermal conditions from no hydrothermal to 6h, resulting in sorbents with three different phases from amorphous to semi-crystalline and crystalline structure. The adsorption isotherms of these adsorbents were found to be well described by the Langmuir isotherm. For the kinetic model, the SP-TSi-1h and the commercial resin are better described by the pseudo-first-order model while the SP-TSi-6h $\Delta$  and LP-TSi-6h $\Delta$  agree with the pseudo-second order model.

Sorbent with the highest crystallinity and longest hydrothermal synthesis (LP-TSi-6h $\Delta$ ) displayed the smallest Pb adsorption capacity and also slow kinetics of adsorption, which is probably the result of rigid crystallinity that hinders the ion-exchange between the Na in the crystalline structure and the Pb ions in the solution. Sorbent with amorphous structure (SP-TSi-1h) shows both the highest capacity and high affinity for Pb due probably to the loosely packed amorphous structure. Sodium ions are well released for exchange with the lead ions.

Ion-exchange between Pb and Na is demonstrated to be the dominant adsorption mechanism, as the Pb adsorption capacity shows a high correlation to the amount of sodium released. Our synthesized titanosilicate can effectively be used for removal of Pb from aqueous solution with the maximum adsorption capacity of about 473 mg/g. After five cycles of regeneration by using NaOH, the adsorption capacities of these adsorbents decreased 20-50% of the initial values.

## References

1. Lidsky, T.I. and J.S. Schneider, *Lead neurotoxicity in children: basic mechanisms and clinical correlates*. Brain, 2003. **126**(1): p. 5-19.
2. Tong, S., Y.E.v. Schirnding, and T. Prapamontol, *Environmental lead exposure: a public health problem of global dimensions*. Bulletin of the World Health Organization, 2000. **78**(9): p. 1068-1077.
3. Notification the Ministry of Science, T.a.E., *Industrial Effluent Standards*, P.C. Department, Editor. 1996, the Royal Government Gazette.
4. Barakat, M.A., *New trends in removing heavy metals from industrial wastewater*. Arabian Journal of Chemistry, 2011. **4**(4): p. 361-377.
5. Fu, F. and Q. Wang, *Removal of heavy metal ions from wastewaters: A review*. Journal of Environmental Management, 2011. **92**(3): p. 407-418.
6. Leinonen, H., *Removal of harmful metals from metal plating waste waters using selective ion exchangers*. 1999: University of Helsinki.
7. Lv, L., et al., *Competitive adsorption of  $Pb^{2+}$ ,  $Cu^{2+}$ , and  $Cd^{2+}$  ions on microporous titanosilicate ETS-10*. J Colloid Interface Sci, 2005. **287**(1): p. 178-84.
8. Faghihian, H., et al., *Synthesis of a novel magnetic zeolite nanocomposite for removal of  $Cs^+$  and  $Sr^{2+}$  from aqueous solution: Kinetic, equilibrium, and thermodynamic studies*. Journal of Colloid and Interface Science, 2013. **393**: p. 445-451.
9. Peng, G.-W. and H.-S. Liu, *FT-IR and XRD characterization of phase transformation of heat-treated synthetic natasite ( $Na_2TiOSiO_4$ ) powder*. Materials Chemistry and Physics, 1995. **42**(4): p. 264-275.
10. Environmental Protection Agency. *Lead*. 2015 [cited 2015 11]; Available from: <http://www2.epa.gov/lead>.
11. García-Lestón, J., et al., *Genotoxic effects of lead: An updated review*. Environment International, 2010. **36**(6): p. 623-636.
12. Agency for Toxic Substances and Disease Registry (ATSDR). *CHEMICAL AND PHYSICAL INFORMATION*. 2015 [cited 2015 11]; Available from: [www.atsdr.cdc.gov/toxprofiles/tp13-c4.pdf](http://www.atsdr.cdc.gov/toxprofiles/tp13-c4.pdf).

13. Environmental Protection Agency. *The Great Lakes*. 2015 [cited 2015 11]; Available from: <http://www.epa.gov/glnpo/atlas/glat-ch4.html#1>.
14. Wayne G. Landis, M.-H.Y., *Introduction to Environmental Toxicology*. 3 ed. 2004. 484.
15. Shahid, M., E. Pinelli, and C. Dumat, *Review of Pb availability and toxicity to plants in relation with metal speciation; role of synthetic and natural organic ligands*. *Journal of Hazardous Materials*, 2012. **219–220**: p. 1-12.
16. De Temmerman, L., et al., *Accumulation of atmospheric deposition of As, Cd and Pb by bush bean plants*. *Environmental Pollution*, 2015. **199**: p. 83-88.
17. Yongsheng, W., L. Qihui, and T. Qian, *Effect of Pb on growth, accumulation and quality component of tea plant*. *Procedia Engineering*, 2011. **18**: p. 214-219.
18. El-Moselhy, K.M., et al., *Bioaccumulation of heavy metals in some tissues of fish in the Red Sea, Egypt*. *Egyptian Journal of Basic and Applied Sciences*, 2014. **1(2)**: p. 97-105.
19. Kwok, C.K., et al., *Bioaccumulation of heavy metals in fish and Ardeid at Pearl River Estuary, China*. *Ecotoxicology and Environmental Safety*, 2014. **106**: p. 62-67.
20. Hildebrand, M.P., *Lead Toxicity in a Newborn*. *Journal of Pediatric Health Care*, 2011. **25(5)**: p. 328-331.
21. Silbergeld, E.K., *Facilitative mechanisms of lead as a carcinogen*. *Mutation Research/Fundamental and Molecular Mechanisms of Mutagenesis*, 2003. **533(1–2)**: p. 121-133.
22. Watch, H.R. *Human Rights Violations in Thailand*. 2014 [cited 2015 15]; Available from: <http://humanrightsviolationsthailand.weebly.com/klity-creek-contamination.html>.
23. guardian, T. *Thai government censured for failure to tackle lead pollution*. 2014 [cited 2015 15]; Available from: <http://www.theguardian.com/global-development/2014/dec/19/thai-government-censured-for-failure-to-tackle-lead-pollution>.
24. Registry, A.f.T.S.a.D. *Lead Toxicity*. 2012 [cited 2014 12]; Available from: <http://www.atsdr.cdc.gov/csem/csem.asp?csem=7&po=8>.

25. Largitte, L., et al., *Comparison of the adsorption of lead by activated carbons from three lignocellulosic precursors*. *Microporous and Mesoporous Materials*, 2016. **219**: p. 265-275.
26. Zhuang, F., et al., *Monodisperse magnetic hydroxyapatite/Fe<sub>3</sub>O<sub>4</sub> microspheres for removal of lead(II) from aqueous solution*. *Journal of Alloys and Compounds*, 2015. **637**: p. 531-537.
27. Arancibia-Miranda, N., et al., *Nanoscale zero valent supported by Zeolite and Montmorillonite: Template effect of the removal of lead ion from an aqueous solution*. *Journal of Hazardous Materials*, 2016. **301**: p. 371-380.
28. Mohan, D., et al., *Lead sorptive removal using magnetic and nonmagnetic fast pyrolysis energy cane biochars*. *Journal of Colloid and Interface Science*, 2015. **448**: p. 238-250.
29. Kang, D., et al., *One-step fabrication and characterization of hierarchical MgFe<sub>2</sub>O<sub>4</sub> microspheres and their application for lead removal*. *Microporous and Mesoporous Materials*, 2015. **207**: p. 170-178.
30. Pandey, P.K., S.K. Sharma, and S.S. Sambhi, *Removal of lead(II) from waste water on zeolite-NaX*. *Journal of Environmental Chemical Engineering*, 2015. **3**(4, Part A): p. 2604-2610.
31. Shahat, A., et al., *Large-pore diameter nano-adsorbent and its application for rapid lead(II) detection and removal from aqueous media*. *Chemical Engineering Journal*, 2015. **273**: p. 286-295.
32. Singh, C.K., et al., *Studies on the removal of Pb(II) from wastewater by activated carbon developed from Tamarind wood activated with sulphuric acid*. *Journal of Hazardous Materials*, 2008. **153**(1-2): p. 221-228.
33. Alijani, H., et al., *A new approach for one step synthesis of magnetic carbon nanotubes/diatomite earth composite by chemical vapor deposition method: Application for removal of lead ions*. *Chemical Engineering Journal*, 2014. **253**: p. 456-463.
34. Sreejalekshmi, K.G., K.A. Krishnan, and T.S. Anirudhan, *Adsorption of Pb(II) and Pb(II)-citric acid on sawdust activated carbon: Kinetic and equilibrium isotherm studies*. *Journal of Hazardous Materials*, 2009. **161**(2-3): p. 1506-1513.

35. Zhou, G., et al., *Sponge-like polysiloxane-graphene oxide gel as a highly efficient and renewable adsorbent for lead and cadmium metals removal from wastewater*. Chemical Engineering Journal, 2015. **280**: p. 275-282.
36. El-Toni, A.M., et al., *Simple and facile synthesis of amino functionalized hollow core–mesoporous shell silica spheres using anionic surfactant for Pb(II), Cd(II), and Zn(II) adsorption and recovery*. Chemical Engineering Journal, 2014. **251**: p. 441-451.
37. Bartczak, P., et al., *Removal of nickel(II) and lead(II) ions from aqueous solution using peat as a low-cost adsorbent: A kinetic and equilibrium study*. Arabian Journal of Chemistry.
38. Jahangiri, M., et al., *The removal of lead ions from aqueous solutions by modified multi-walled carbon nanotubes with 1-isatin-3-thiosemicarbazone*. Journal of Molecular Liquids, 2015. **212**: p. 219-226.
39. Zhou, Y., et al., *Use of carboxylated cellulose nanofibrils-filled magnetic chitosan hydrogel beads as adsorbents for Pb(II)*. Carbohydrate Polymers, 2014. **101**: p. 75-82.
40. Zhu, Y., et al., *Highly efficient adsorption of Hg(II) and Pb(II) onto chitosan-based granular adsorbent containing thiourea groups*. Journal of Water Process Engineering, 2015. **7**: p. 218-226.
41. Lee, C.-G., et al., *Lead and copper removal from aqueous solutions using carbon foam derived from phenol resin*. Chemosphere, 2015. **130**: p. 59-65.
42. Geetha, P., et al., *Nanoalginate based biosorbent for the removal of lead ions from aqueous solutions: Equilibrium and kinetic studies*. Ecotoxicology and Environmental Safety, 2015. **122**: p. 17-23.
43. Seifpanahi Shabani, K., et al., *Preparation and characterization of novel nano-mineral for the removal of several heavy metals from aqueous solution: Batch and continuous systems*. Arabian Journal of Chemistry.
44. Guo, X., et al., *Synthesis of amino functionalized magnetic graphenes composite material and its application to remove Cr(VI), Pb(II), Hg(II), Cd(II) and Ni(II) from contaminated water*. Journal of Hazardous Materials, 2014. **278**: p. 211-220.



45. Husing, U.S.a.N., *Synthesis of Inorganic Materials*. 3 ed. 2012: WILEY-VCH Verlag GmH&Co.HGaA. 392
46. Araki, S., et al., *Crystallization process of zeolite rho prepared by hydrothermal synthesis using 18-crown-6 ether as organic template*. Journal of Colloid and Interface Science, 2012. **376**(1): p. 28-33.
47. Ismail, N., I.H. Abd El-Maksod, and H. Ezzat, *Synthesis and characterization of titanosilicates from white sand silica and its hydrogen uptake*. International Journal of Hydrogen Energy, 2010. **35**(19): p. 10359-10365.
48. Rocha, J., et al., *Synthesis of microporous titanosilicate ETS-10 from TiCl<sub>3</sub> and TiO<sub>2</sub>: a comprehensive study*. Microporous and Mesoporous Materials, 1998. **23**(5–6): p. 253-263.
49. Pavel, C.C., et al., *Synthesis and characterization of the microporous titanosilicates ETS-4 and ETS-10*. Microporous and Mesoporous Materials, 2002. **56**(2): p. 227-239.
50. Ji, Z., et al., *Hydrothermal synthesis of titanosilicate ETS-10 using Ti(SO<sub>4</sub>)<sub>2</sub>*. Microporous and Mesoporous Materials, 2005. **81**(1–3): p. 1-10.
51. Kostov-Kytin, V., et al., *Hydrothermal synthesis of microporous titanosilicates*. Microporous and Mesoporous Materials, 2007. **105**(3): p. 232-238.
52. LEWATIT, *product information*. 2010.
53. Hassan, A.F., A.M. Abdel-Mohsen, and M.M.G. Fouda, *Comparative study of calcium alginate, activated carbon, and their composite beads on methylene blue adsorption*. Carbohydrate Polymers, 2014. **102**: p. 192-198.
54. Limousin, G., et al., *Sorption isotherms: A review on physical bases, modeling and measurement*. Applied Geochemistry, 2007. **22**(2): p. 249-275.
55. Dada, A., et al., *Langmuir, Freundlich, Temkin and Dubinin–Radushkevich isotherms studies of equilibrium sorption of Zn<sup>2+</sup> unto phosphoric acid modified rice husk*. Journal of Applied Chemistry, 2012. **3**(1): p. 38-45.
56. Ho, Y.-S., *Isotherms for the sorption of lead onto peat: comparison of linear and non-linear methods*. Polish Journal of Environmental Studies, 2006. **15**(1): p. 81-86.
57. Foo, K.Y. and B.H. Hameed, *Insights into the modeling of adsorption isotherm systems*. Chemical Engineering Journal, 2010. **156**(1): p. 2-10.

58. Salimpour Abkenar, S., R.M.A. Malek, and F. Mazaheri, *Dye adsorption of cotton fabric grafted with PPI dendrimers: Isotherm and kinetic studies*. Journal of Environmental Management, 2015. **163**: p. 53-61.
59. Hutson, N.D. and R.T. Yang, *Theoretical basis for the Dubinin-Radushkevitch (DR) adsorption isotherm equation*. Adsorption, 1997. **3**(3): p. 189-195.
60. Donat, R., et al., *Thermodynamics of Pb<sup>2+</sup> and Ni<sup>2+</sup> adsorption onto natural bentonite from aqueous solutions*. Journal of Colloid and Interface Science, 2005. **286**(1): p. 43-52.
61. Karapinar, N. and R. Donat, *Adsorption behaviour of Cu<sup>2+</sup> and Cd<sup>2+</sup> onto natural bentonite*. Desalination, 2009. **249**(1): p. 123-129.
62. Arshadi, M., M.J. Amiri, and S. Mousavi, *Kinetic, equilibrium and thermodynamic investigations of Ni(II), Cd(II), Cu(II) and Co(II) adsorption on barley straw ash*. Water Resources and Industry, 2014. **6**: p. 1-17.
63. Lin, J. and L. Wang, *Comparison between linear and non-linear forms of pseudo-first-order and pseudo-second-order adsorption kinetic models for the removal of methylene blue by activated carbon*. Frontiers of Environmental Science & Engineering in China, 2009. **3**(3): p. 320-324.
64. Qiu, H., et al., *Critical review in adsorption kinetic models*. Journal of Zhejiang University Science A, 2009. **10**(5): p. 716-724.
65. Hameed, B.H., I.A.W. Tan, and A.L. Ahmad, *Adsorption isotherm, kinetic modeling and mechanism of 2,4,6-trichlorophenol on coconut husk-based activated carbon*. Chemical Engineering Journal, 2008. **144**(2): p. 235-244.
66. Liu, W., et al., *Adsorption of Cu(II) and Cd(II) on titanate nanomaterials synthesized via hydrothermal method under different NaOH concentrations: Role of sodium content*. Colloids and Surfaces A: Physicochemical and Engineering Aspects, 2014. **452**(0): p. 138-147.